

Light Water Reactor Sustainability Program

Assessment of Modeling and Simulation Technical Gaps in Safety Analysis of High-Burnup Accident-Tolerant Fuels



January 2023

U.S. Department of Energy

Office of Nuclear Energy

DISCLAIMER

This information was prepared as an account of work sponsored by an agency of the U.S. Government. Neither the U.S. Government nor any agency thereof, nor any of their employees, makes any warranty, expressed or implied, or assumes any legal liability or responsibility for the accuracy, completeness, or usefulness, of any information, apparatus, product, or process disclosed, or represents that its use would not infringe privately owned rights. References herein to any specific commercial product, process, or service by trade name, trademark, manufacturer, or otherwise, does not necessarily constitute or imply its endorsement, recommendation, or favoring by the U.S. Government or any agency thereof. The views and opinions of authors expressed herein do not necessarily state or reflect those of the U.S. Government or any agency thereof.

Assessment of Modeling and Simulation Technical Gaps in Safety Analysis of High-Burnup Accident- Tolerant Fuels

**Sujong Yoon
Carlo Parisi
Yong-Joon Choi**

Idaho National Laboratory

January 2023

**Prepared for the
U.S. Department of Energy
Office of Nuclear Energy**

Page intentionally left blank

EXECUTIVE SUMMARY

The United States nuclear industry is facing a strong challenge to maintain regulatory-required levels of safety while ensuring economic competitiveness to stay in business. Safety remains a key parameter for all aspects related to the operation of light water reactor (LWR) nuclear power plants (NPPs), and it can be achieved more economically by using a risk-informed ecosystem, such as that being developed by the Risk-Informed Systems Analysis (RISA) Pathway under the U.S. Department of Energy (DOE) Light Water Reactor Sustainability (LWRS) Program. The LWRS Program is promoting a wide range of research and development activities to maximize both the safety and economically efficient performance of NPPs through improved scientific understanding, especially given that many plants are considering second license renewal.

The RISA Pathway has two main goals:

- The deployment of methodologies and technologies that enable better representation of safety margins and the factors that contribute to cost and safety, and
- The development of advanced applications that enable cost-effective plant operation.

As part of the RISA Pathway, the Enhanced Resilient Plant (ERP) project refers to an NPP where safety is improved by implementing various measures, such as accident-tolerant fuels (ATF), diverse and flexible coping strategy (FLEX), enhancements to plant components and systems, incorporation of augmented or new passive cooling systems, and utilization of advanced battery technologies. The objective of the ERP research is to use novel methods and computational tools to enhance existing reactors' safety while reducing operational costs.

Many U.S. utilities are targeting implementation of ATFs instead of traditional fuel in the near future since ATFs offer benefits in terms of improved performance and cost savings. The robust properties of ATF make it possible to extend the refueling cycle from 18 to 24 months in addition to the opportunity to use less of fuel. Extensive safety assessments are required to support regulatory requirements and obtain the approvals to use ATFs and the ERP project support the industry by developing novel effective methodologies for safety evaluations. In this project, the technical gaps in the modeling and simulation of the high burnup (HBU) ATF were assessed in terms of the fuel cladding behavior during the postulated accident events. The issues were identified in modeling the cladding deformation, the hydrodynamic change due to cladding deformation and the critical heat flux (CHF). The RELAP5-3D cladding deformation model was assessed by multiple verification tests and validation with the instrumented fuel assembly (IFA) experiment.

Page intentionally left blank

CONTENTS

1.	INTRODUCTION	11
2.	ASSESSMENT OF TECHNICAL GAPS IN MODELING AND SIMULATION OF HBU ATF SAFETY ANALYSIS	12
2.1	Overview of the Cladding Deformation Mechanism	12
2.2	Technical Issues in High-Burnup Accident-Tolerant Fuel Safety Analysis	14
2.2.1	Gaps in Data and Simulation Tools	14
2.2.2	Issues in Modeling and Simulation	15
2.2.2.1	Cladding Deformation	15
2.2.2.2	Multi-Dimensional Flow in the Core	16
2.2.2.3	Critical Heat Flux	17
3.	ASSESSMENT OF THE RELAP5-3D CLADDING DEFORMATION MODEL	18
3.1	Review on the RELAP5-3D Cladding Deformation Model	18
3.2	Verification Test of RELAP5-3D Cladding Deformation Model	20
3.2.1	Model Description	20
3.2.2	Results of the Verification Tests	21
3.2.2.1	Ramp Temperature 1 K/sec	22
3.2.2.2	Ramp Temperature 5 K/sec	23
3.2.2.3	Ramp Temperature 15 K/sec	24
3.2.2.4	Ramp Temperature 27 K/sec	24
3.2.3	Sensitivity Study on the Time Step Size	25
3.3	Validation of the RELAP5-3D Cladding Deformation Model	27
3.3.1	Summary of Halden IFA-650 Experiments	27
3.3.2	Description on the IFA-650.10 Test	28
3.3.2.1	IFA-650.10 Test Rig Geometry	28
3.3.2.2	Data from the IFA-650.10 Test	30
3.3.3	RELAP5-3D Simulation of the IFA-650.10 Test	31
3.3.3.1	RELAP5-3D Nodalization	31
3.3.3.2	RELAP5-3D Simulation Result	34
3.3.4	Data Comparison and Discussion	35
4.	CONCLUSION AND REMARK	39
5.	REFERENCES	40

FIGURES

Figure 1. Zr cladding fuel rod behavior during a double-ended cold leg break LBLOCA [3].	12
Figure 2. Fuel cladding deformation mechanism during LOCA [4].	13
Figure 3. Zr cladding hoop stress correlation in water coolant [6].	13
Figure 4. The overview of Halden IFA-650 LOCA test series [7].	14
Figure 5. Hoop stress of Cr-coated Zr cladding behavior during three cycles of operation [25].	16
Figure 6. Cladding deformation during the PHEBUS experiment [27].	17
Figure 7. RELAP5-3D nodalization for the cladding deformation test case.	21
Figure 8. RELAP5-3D fuel rod nodalization and dimension.	21
Figure 9. Cladding radius and gap width behavior at Node 6 in the 1 K/sec case.	22
Figure 10. Cladding temperature and rod internal pressure behavior at Node 6 in the 1 K/sec case.	22
Figure 11. Cladding radius and gap width behavior at Node 6 in the 5 K/sec case.	23
Figure 12. Cladding temperature and rod internal pressure behavior at Node 6 in the 5 K/sec case.	23
Figure 13. Cladding radius and gap width behavior at Node 6 in the 15 K/sec case.	24
Figure 14. Cladding temperature and rod internal pressure behavior at Node 6 in the 15 K/sec case.	24
Figure 15. Cladding radius and gap width behavior at Node 6 in the 27 K/sec case.	25
Figure 16. Cladding temperature and rod internal pressure behavior at Node 6 in the 27 K/sec case.	25
Figure 17. Cladding temperature behavior at Node 6 with different time step sizes.	26
Figure 18. Rod internal pressure behavior at Node 6 with different time step sizes.	26
Figure 19. Gap width behavior at Node 6 with different time step sizes.	27
Figure 20. Mass error behavior at Node 6 with different time step sizes.	27
Figure 21. Schematic of the IFA-650.10 LOCA test rig with instrument elevations [8].	28
Figure 22. Cross-sectional geometry of the IFA-650.10 rig [8].	29
Figure 23. Axial power profile at the beginning of test of IFA-650.10 [8].	29
Figure 24. IFA-650.10 Experiment Data Set 1: Temperatures of cladding (TCC), heater (TCH), coolant inlet (TIA) and outlet (TOA) temperatures, and heater power (Heater LHR) [7].	31
Figure 25. IFA-650.10 Experiment Data Set 2: Rod internal pressure (PF1), cladding temperature (TCC1), rod elongation (EC2), and gamma monitor response in the blowdown line (MON40) [7].	31
Figure 26. RELAP5-3D nodalization of IFA-650.10.	32
Figure 27. Detailed nodalization of core section of IFA-650.10 test section.	33
Figure 28. Temperature and pressure behavior at Node 14 of RELAP5-3D IFA-650.10 simulation.	34
Figure 29. Temperature and pressure behavior at Node 14 of RELAP5-3D IFA-650.10 simulation (power adjusted).	35

Figure 30. Lower elevation cladding (TCC1 and Node 6) cladding temperatures comparison..... 36

Figure 31. Higher elevation cladding (TCC2 and Node 18) cladding temperatures comparison. 36

Figure 32. Comparison of burst position using cladding outer diameter. 37

Figure 33. Comparison of the rod internal pressure..... 37

Figure 34. RELAP5-3D rod internal pressure comparison with different reference volume. 38

TABLES

Table 1. Zr cladding deformation model look-up table [6]..... 19

Table 2. Major design parameters of the IFA-650.10 test rig [8]. 30

Table 3. Time sequence of the IFA-650.10 RELAP5-3D simulation result. 35

ACRONYMS

ATF	accident-tolerant fuel
BWR	boiling-water reactor
CHF	critical heat flux
DBA	design basis accident
DNBR	departure nucleate boiling rate
DOE	Department of Energy
ECCS	emergency core cooling system
ERP	Enhanced Resilient Power plant
FFRD	fuel fragmentation, relocation and dispersal
FLEX	Diverse and Flexible Coping Strategy
FY	fiscal year
HBU	high burnup
IFA	instrumented fuel assembly
INL	Idaho National Laboratory
LBLOCA	large-break loss-of-coolant accident
LOCA	loss-of-coolant accident
LWR	light-water reactor
LWRS	Light Water Reactor Sustainability
NPP	nuclear power plant
NRC	U.S. Nuclear Regulatory Commission
NUREG	Nuclear Regulatory Report
OECD	Organization for Economic Cooperation and Development
PCMI	pellet-cladding mechanical interaction
PCT	peak cladding temperature
PWR	pressurized-water reactor
RIA	reactivity-initiated accident
RISA	Risk-Informed System Analysis
U.S.	United States

1. INTRODUCTION

The United States (U.S.) Department of Energy (DOE) Light Water Reactor Sustainability (LWRS) Program Risk-Informed Systems Analysis (RISA) Pathway Enhanced Resilient Plant (ERP) aims to enhance both the safety and economics of existing nuclear power plants (NPPs) using advanced, near-term technologies that provide substantial improvements to plant safety margins. The project supports the DOE and industry initiatives targeting improvements of the safety and economic performance of the current fleet of NPPs such as accident-tolerant fuel (ATF), diverse and flexible coping strategy (FLEX), passive cooling system designs, and advanced battery technologies. The ERP concept refers to an NPP where safety is improved by implementing various measures, such as those described in the previous sentence. The objective of the ERP research is to use novel methods and computational tools to enhance existing reactors' safety while reducing operational costs. From Fiscal Year 2022, the project is focusing on the safety assessments of ATFs with increased enrichment and extended burnup (i.e., high burnup), which is an urgent near-term industry initiative that offers safety enhancements as well as economic gains [1]. This work could serve as a roadmap for safety analyses that NPPs must include in their license amendment requests supporting the use of ATFs.

The possibility of higher burnup is more achievable with ATF compared to the traditional Zr-clad fuel due to ATF's more robust cladding properties to cope with accident conditions. In this context, extended high burnup (HBU) operation up to 24 months can provide a significant economic benefit for operating nuclear reactors. However, ATF development is still ongoing along with the enhancement of the modeling and simulation capabilities that can provide sufficient information about how HBU ATF performs under accident scenarios. The safety analyses of HBU ATF is still incomplete, especially in terms of fuel performance. The fuel cladding failure could occur during postulated accident events and may cause fuel damage exceeding the regulation safety limits. The main limiting degradation phenomena are the cladding deformation and fuel fragmentation, relocation, and dispersal (FFRD). The cladding deformation is possible during a loss-of-coolant accident (LOCA). A large pressure difference between the fuel rod internals and externals may cause fuel cladding ballooning (or swelling) and eventually a burst¹. For the FFRD, the ceramic fuel (i.e., UO₂) starts making random fractures and pulverizes into small particles, which is called fuel fragmentation. As burnup increased, the fuel fragment size becomes smaller. These fragments can be relocated to the bottom of the fuel rod or stacked where the fuel rod has deformed. When cladding bursts, the fuel fragments can be dispersed into the reactor core or to the environment. For this reason, understanding the correct fuel failure mechanism is one of most important parameters for the fuel licensing, which needs to include both fuel performance and system safety analyses. However, there is a large technical gap in fuel performance and system safety analyses for the HBU ATF since previous studies have been largely focused on the Zr-based cladding fuels. Therefore, the RISA Pathway initiated a task to assess technical gaps in the modeling and simulation of the HBU ATF fuel failure and relevant safety analyses.

As the first step of the activity, technical gaps in the modeling and simulation of the reactor systems loaded with HBU ATF were assessed by focusing on the RELAP5-3D cladding deformation model, a unique feature among the available system analysis tools. The verification and validation was also performed for the cladding deformation model in RELAP5-3D to identify research needs. The work will continue to improve the relevant physical models in RELAP5-3D, which will support developing industrial grade modeling and simulation tools for HBU ATF safety analyses. An investigation will be also performed for possible risk-informed approaches to demonstrate HBU ATF safety margin management. The project will continue collaboration with DOE's Advanced Fuel Campaign program, which is currently focused on performing experimental testing of HBU ATF in Idaho National Laboratory's Transient Reactor Test Facility (i.e., TREAT).

¹ The term "rupture" is used in the RELAP5-3D manual; however, the correct term is "burst," as shown in Figure 2.

2. ASSESSMENT OF TECHNICAL GAPS IN MODELING AND SIMULATION OF HBU ATF SAFETY ANALYSIS

2.1 Overview of the Cladding Deformation Mechanism

Initially, the pressurized-water reactor (PWR) fuel rod internal pressure is set about 2 MPa from the manufacturer to maintain integrity during the normal reactor operation at a high pressure of 15.5 MPa. As burnup increases, the rod internal pressure increases up to 6 MPa at a 60 GWD/MTU burnup [2]. During a LOCA event, the reactor pressure drops close to ambient (i.e., 0.1 MPa) as the coolant flushed out through the broken pipe. The difference between the fuel rod internal and external pressure is the main reason for the fuel failure due to cladding deformations: ballooning and burst.

Figure 1 shows cladding temperature and system pressure behavior during a double-ended cold leg break large-break LOCA (LBLOCA). The figure indicates three regimes that occur over the course of a LOCA: blowdown, refill, and reflood. Once blowdown occurred due to the cold leg rupture, the emergency core cooling system (ECCS) will be automatically activated. At this point, the fuel temperature may fluctuate due to rewet. However, cooling of the reactor fuel will be unsettled until the reactor core is refilled, and the cladding temperature will rise from the decay heat of the nuclear fuel. In this sequence, fuel could be damaged by the plastic deformation of the cladding, mainly from the pressure difference across the fuel cladding. If the fuel peaking factor has a high rating (e.g., $F_q=2.5$), the cladding could be deformed in the reflooding stage.

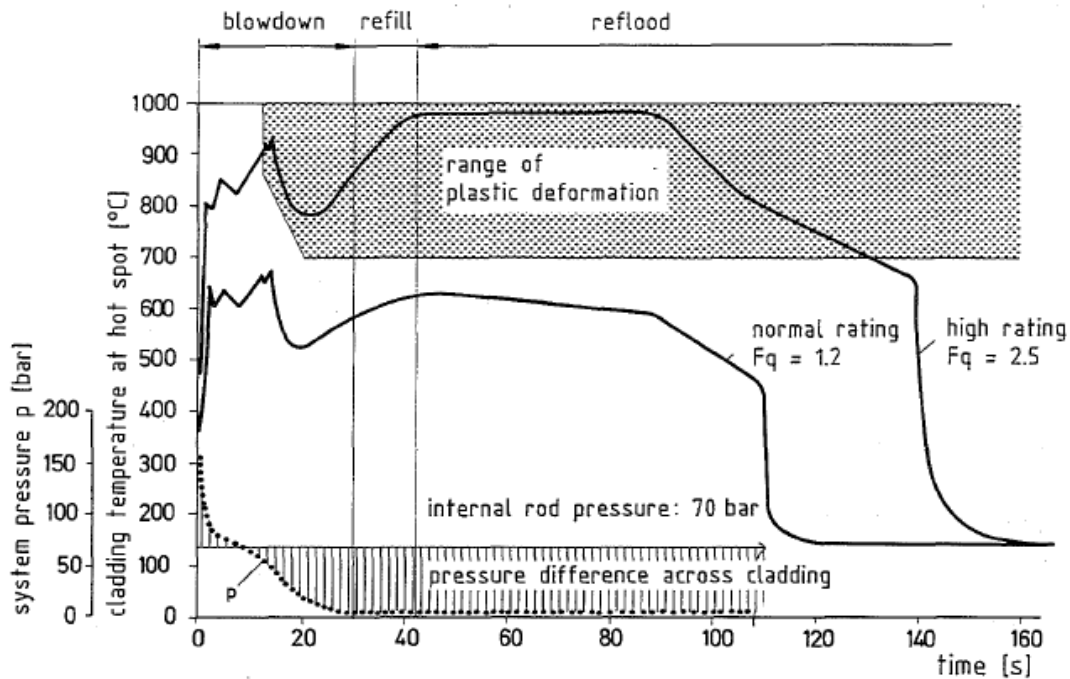


Figure 1. Zr cladding fuel rod behavior during a double-ended cold leg break LBLOCA [3].

Figure 2 shows the mechanism of the cladding deformation during a LOCA event. In general, the cladding starts ballooning around 30 seconds and burst occurs around 50 seconds from the blowdown phase which makes coolant blockage. The cladding temperature continuously increases due to the decay heat. The metal-water reaction starts when the cladding temperature reaches around 1000–1200°C. In this high-temperature oxidation range, the equivalent cladding reacted (ECR) point appears which the regulation limit of 17% oxidation rate. The cladding will reach the peak cladding temperature (PCT) and fuel fragments will relocate inside the fuel rod. Once the reflood and cooling continues, cladding may be quenching (i.e., a sudden temperature drop), which can cause fuel rod rupture or total failure.

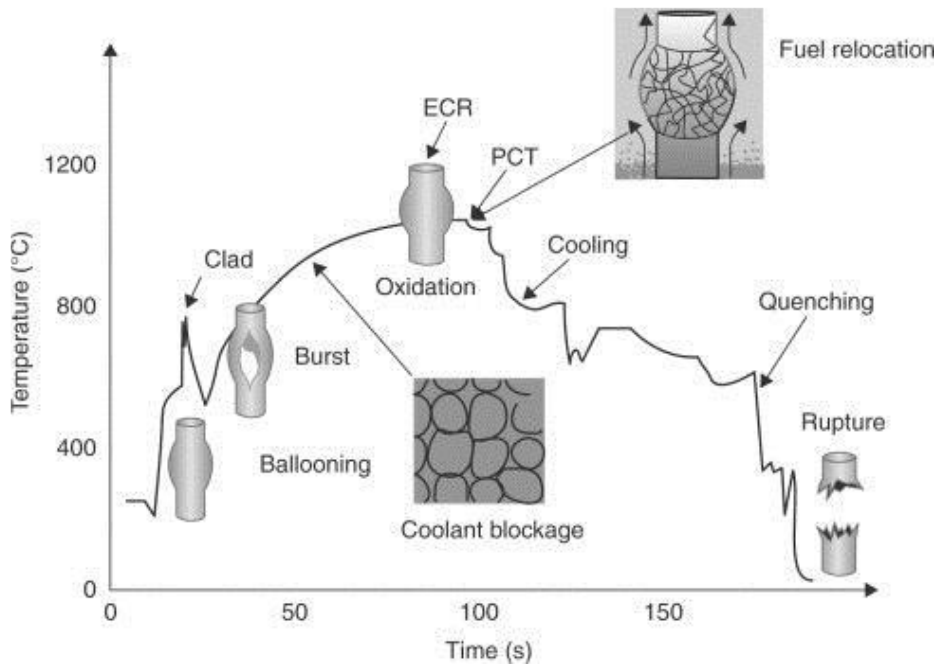


Figure 2. Fuel cladding deformation mechanism during LOCA [4].

The mechanism of cladding deformation is very complex due to mechanical characteristics (e.g., stresses and strains) that vary with temperature, oxidation, irradiation, crystallization, and fission product behavior [5]. Consequently, the behavior of Zr cladding depends strongly on the environment during a LOCA event, but the main cause of the cladding deformation is the pressure difference across the cladding wall and temperature and the exposure duration under accident conditions. The correlation of the cladding deformation was therefore developed in early 1980s based on the hoop stress to remove design-specific dimensional effects from the pressure and temperature [5]. Figure 3 shows the hoop stress correlation as a function of cladding temperature based on various experimental data.

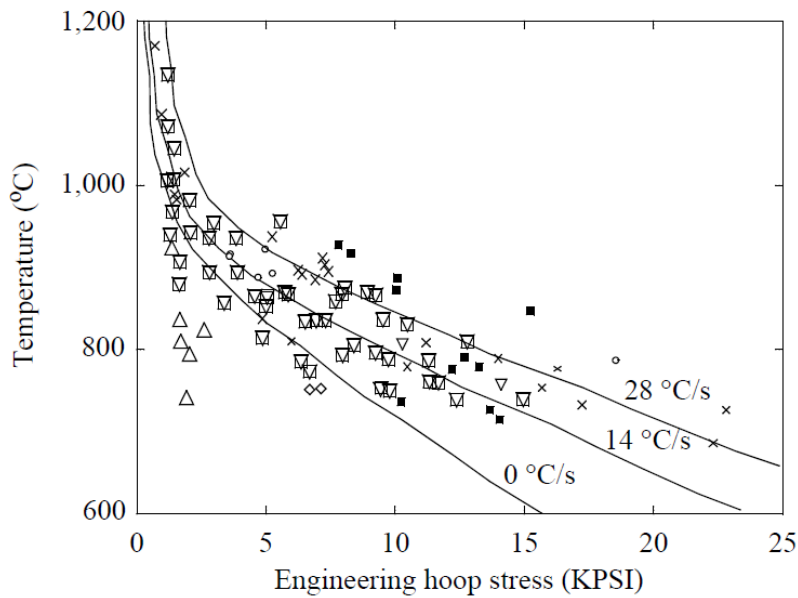


Figure 3. Zr cladding hoop stress correlation in water coolant [6].

The correlation also considers the temperature ramp rate to cover a wide temperature range and reduce experimental uncertainties but is still conservative. As of today, this correlation is widely used worldwide for analyzing Zr-based cladding deformation, including RELAP5-3D.

The major fuel failure phenomena of the HBU ATFs during postulated accidents are similar to those of the Zr cladding fuel: FFRD and cladding deformation. However, the mechanism is different in HBU ATF due to the accident response and behavior. From the Halden reactor experiment, it is clear that the size of fuel fragments becomes smaller at higher burnups, as shown in Figure 4. The smaller fuel particle will easily relocate in the fuel rod and induce fuel failure. The rod internal pressure will also reach higher than Zr cladding fuel in HBU, which will ease cladding deformation [2].

test #	2	7	6	11	10	12	13	14	3	5	9	4
burnup, MWd/kg	0	44.3	55.5	56	60	72.3	74.1	71.1	81.9	83	90	92
balloon strain, %	54	23	49	25	15	40	45	55	8	15	61	62
radio-graphy												
ceramo-graphy							fragment size distribution only	fragment size distribution only				
fragment size	coarse	coarse	coarse	coarse	coarse & some fine	coarse & fine	coarse (& fine?)	coarse (& fine?)	medium & fine	medium & fine	medium & fine	medium & fine
gamma scan												
flask bottom →												
HBS width												
dispersal (qualitative)	none	none	none	none	some	some more	nearly none	did not fail	n/a	much	much more	much more

Figure 4. The overview of Halden IFA-650 LOCA test series [7].

2.2 Technical Issues in High-Burnup Accident-Tolerant Fuel Safety Analysis

2.2.1 Gaps in Data and Simulation Tools

In May 2022, the U.S. Nuclear Regulatory Commission (NRC) published a report to identify regulatory needs and technical guidance for the near-term ATF concepts (Cr-coated Zr with doped UO₂) with a HBU (up to 68 and 75 GWD/MTU) and increased enrichment beyond 5.0 wt% [9]. The NRC report concluded that the current regulation guides need to be revised for licensing HBU ATFs due to the lack of technical basis in terms of both cladding deformation and FFRD. The main data gaps were identified for the cladding strain limits, cladding axial growth, oxide thickness, hydrogen concentration, fission gas data, source term, and rod internal pressure. For the accident analysis, the data are missing for cladding embrittlement behavior during LOCA,

cladding failure mechanism during a reactivity-initiated accident (RIA), and fuel dispersal characteristics in all design basis accidents (DBAs) [10]. Especially for the LOCA analysis of HBU fuels, new experiments are necessary to collect data related to (1) HBU fuel rod conditions before LOCA, (2) definition of LOCA conditions of HBU fuels, (3) discrepancy between experiment and commercial HBU LOCA analysis, and (4) HBU fuels cladding deformation and FFRD data [10]. The Phenomena Identification and Ranking Tables (i.e., PIRT) method was also used to weight the importance of the data gaps in the HBU and ATF safety analyses based on the amount of fission products released into the containment and quantity of combustible gases generated during an accident as the figures-of-merit [12].

The ATFs are designed to lower the hydrogen generation rates. The less oxidation of the cladding material can improve plant resiliency during the postulated accidents. For the ATFs, the most concerning DBA is the RIA in terms of the fuel failure. The rapid increase of the reactivity (more than 1,000 times than normal) in a very short period (about 20 ms) can cause a fuel pellet-cladding mechanical interaction, which increases the cladding hoop strain at a relatively lower temperature (<700°C). The fuel cladding will balloon and eventually burst. Especially for the HBU, the pulverized fuel size is very small and the fragmentation rate will be high. The rod internal pressure will be higher than lower burnup fuels as well. For this reason, a RIA can easily develop fuel failure in HBU ATF. The OECD Nuclear Energy Agency recently identified experiment needs and conditions for RIA based on the transient pulse, which will decide the pellet-cladding mechanical interaction failure rate [13]. Idaho National Laboratory also prepared a series of RIA experiments for the HBU ATF to develop fuel performance data over 60 GWD/MTU [14].

RIA modeling and simulation is quite complex since RIA is a combination of neutron physics, thermal-hydraulics, and fuel performance. RELAP5-3D is able to simulate both thermal-hydraulics and reactor kinetics in multiple dimensions (e.g., point and nodal reactor kinetics). Based on the NESTLE neutronics code, RELAP5-3D can solve multigroup nodal kinetics in multiple dimensions [6]. Thus, RELAP5-3D can accurately simulate rapid reactivity change and thermal-hydraulics feedback to the entire nuclear system. The finite-element-based nuclear fuel performance code BISON [15] was coupled with RELAP5-3D to simulate RIA of Zr cladding fuel in TREAT facility [16]. The simulation focused on the prediction of the fuel failure over a range of transient pulse width. RELAP5-3D coupled with BISON provides thermal-hydraulics feedback to the mechanical effects on the fuel-to-cladding gap conductance, cladding-to-coolant heat transfer coefficient, temperature and pressure.

Since BISON is a high-fidelity code and needs large computational resources, lighter but faster fuel performance tools have been coupled with RELAP5 series. The MARS-KS, the Korean system code based on RELAP5/MOD3, has been coupled with FRAPTRAN, the fuel rod analysis program transient code from the US NRC [17]. The research progressed to model fuel fragmentation and relocation and improve the Zr cladding deformation model during the LOCA. The RISA Pathway also developed a coupling interface between RELAP5-3D and the TRANSURANUS fuel performance code by using the Risk Analysis and Virtual ENvironment (RAVEN) code, which allows risk-informed multi-physics uncertainty analyses [18].

For the ATF metal-water reaction model, many system codes have already been updated. RELAP5-3D has been updated to model FeCrAl (Kanthal) and Cr-coated Zr [25]. TRACE and MELCOR codes can model FeCrAl, and the MAAP code can model both SiC and FeCrAl [32]. However, further verification and validation is needed for the ATF metal-water reaction model.

2.2.2 Issues in Modeling and Simulation

2.2.2.1 Cladding Deformation

Unlike Zr or FeCrAl ATF, the Cr-coated Zr cladding has heterogeneous behavior in its material since it has a chromium layer on the Zr cladding surface. One of main issues modeling the Cr-coated Zr cladding is that the hoop stress curve differs with the thickness of the oxide layer, and it is extremely difficult to develop the correlation. Figure 5 clearly shows that the hoop stress curve differs with the thickness of the coating layer [21][22]. This behavior also appears in the other surface-coated Zr claddings [23]. For this reason, high-fidelity computational tools (e.g., BISON) are recommended for such heterogenous ATF performance analyses [24].

Another issue in the cladding deformation model is that a hydrodynamic area change can generate a large mass error during the simulation and cause a numerical instability with a code failure. RELAP5-3D was updated in early 2000s to model a hydrodynamic area change due to the cladding deformation. The outcome of research will be published in the near future.

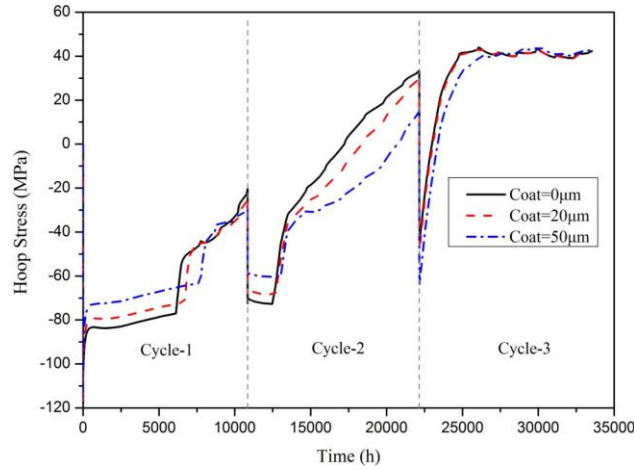


Figure 5. Hoop stress of Cr-coated Zr cladding behavior during three cycles of operation [25].

2.2.2.2 Multi-Dimensional Flow in the Core

In case of RELAP5-3D or other system code simulation, the fuel failure modeling generally uses a single channel flow geometry. If there is forced flow in the system (i.e., the mass flow rate is not zero) to model system cooling or heat loss, the flow area will decrease while fuel cladding swells or balloons. It will make the flow velocity faster if the mass flow rate is constant and will increase the heat transfer from fuel to coolant. This phenomena was observed in the IFA-650.10 test and simulation, which has to be extrapolated to accidental conditions (e.g., the simulation temperature is lower than actual reactor operating conditions). However, this phenomena will not occur at the actual reactor core during the LOCA sequence. As shown in Figure 6, as the vertical flow path is altered due to the cladding deformation, the cross flow will be perpendicular to the axial fuel rod direction.

The heat transfer will only be relying on the natural circulation of the superheated steam and radiation heat transfer after the LOCA blow-out phase. Even at the LOCA refill phase, there will be no forced flow of the system until the ECCS is fully reactivated. Hence, modeling the cladding deformation needs to use at least 5×5 size of sub-channel along with the multi-dimensional flow model to consider cross flow effects [26].

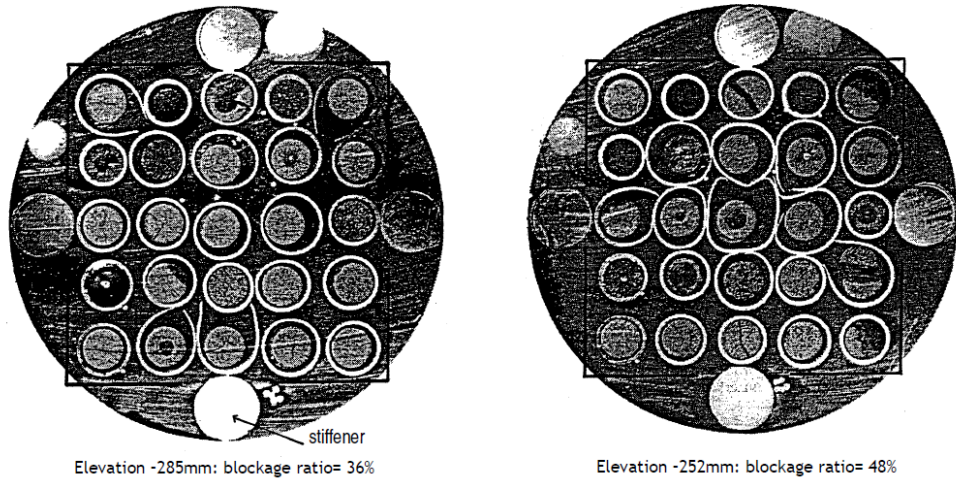


Figure 6. Cladding deformation during the PHEBUS experiment [27].

2.2.2.3 Critical Heat Flux

The critical heat flux (CHF) is an important parameter to determine the operational safety limit of LWRs which restricts the departure nucleate boiling ration (DNBR²) to 1.2. This means the ratio between CHF and design heat flux should be under 1.2 to avoid coolant film boiling which can lead to fuel damage due to a lack of heat transfer from the fuel rod to the coolant. For this reason, correctly calculating the CHF is necessary for DBA analyses, especially for predicting the PCT, which also is a design parameter. The CHF is mainly derived from the look-up tables which is based the experimental correlations [28]. However, current CHF data are based on the Zr cladding. The recent study shows a 10% increase in CHF is available in FeCrAl while no change is foreseen in the Cr-coated Zr cladding [29]. This is an important finding that implies that the reactor power can be increased 10% more than currently while retaining DNBR of 1.2. Current safety analysis tools (e.g., RELAP5-3D) have CHF correlations that may need an update for reproducing the possible increased margin for FeCrAl ATF.

² Minimum critical power ratio in BWR.

3. ASSESSMENT OF THE RELAP5-3D CLADDING DEFORMATION MODEL

The RELAP5-3D cladding deformation originates from the fuel performance analysis code FRAP-T6 [30], which has a theoretical base in NUREG-0630 [5]. The model can simulate the plastic deformations (i.e., ballooning and burst) of the Zr cladding due to the temperature change during the LOCA event. The cladding deformation model for ATFs is not yet developed. The model uses empirical correlations, which informs the user of the possible fuel rod burst and flow blockage rate. Hence, it is recommended that additional detail analyses are necessary using fuel rod simulation tools.

In this chapter, we assessed the RELAP5-3D cladding deformation model toward experimental data. A series of tests was conducted to verify the model and a validation test was performed using the IFA-650.10 fuel performance experiment.

3.1 Review on the RELAP5-3D Cladding Deformation Model

The RELAP5-3D cladding deformation model is an additional term of the dynamic gap conductance model, which calculates the effective gap conductivity based on a simplified deformation model. This model is only valid for Zr cladding under LOCA conditions. When the cladding deformation model is active, the total cladding strain used in the dynamic gap conductance model includes the thermal strain, the creep-down strain, the elastic strain, and the plastic strain. The rod internal pressure and radius of the fuel, gap, and cladding are also calculated from the gap conductance model.

As discussed in the previous chapter, the main trigger of the cladding deformation is the pressure difference between the rod internal and external pressure. However, the RELAP5-3D cladding deformation model only uses predefined hoop stress and burst strain correlations based on the cladding temperature.

A small amount of ballooning can occur in the dynamic gap conductance model. The large balloon size will then occur when the average cladding temperature exceeds the temperature where the plastic strain of Zr cladding begins (T_{plas}), by using the burst temperature (T_b) from the look-up table (Table 1) interpolation.

T_{plas} is calculated from:

$$\begin{aligned} T_{plas} &= T_b - 70^\circ\text{C}; & T_b < 700^\circ\text{C} \\ &= T_b - 70^\circ\text{C} - 0.14(T_b - 700^\circ\text{C}); & 700^\circ\text{C} < T_b < 1300^\circ\text{C} \\ &= T_b - 155^\circ\text{C}; & 1300^\circ\text{C} < T_b \end{aligned}$$

T_b is given by:

$$T_b = 3960^\circ\text{C} - \left(\frac{20.4 \cdot S}{1 + H} \right) - \left[\frac{8.51 \times 10^6 \cdot S}{100(1 + H) + 2790 \cdot S} \right]$$

where,

S = cladding hoop stress (KPSI)

$H = \min[(\text{heating rate})/(28^\circ\text{C/s}), 1.0]$

When a burst occurred, the look-up table (Table 1) was again used to find the burst strain, burst temperature, and flow blockage rate by the linear interpolation. The range of the look-up table is a heating rate between 10 and 25°C/sec. The interpolation is only valid for burst temperatures between 600 and 1200°C. Outside of range will use values from 600 or 1200°C without extrapolation.

The heating rate is calculated from the average cladding temperature at the present time step minus the previous time step's average cladding temperature, which is divided by the time step size. The cladding hoop stress is interpolated from the correlations in Figure 3.

Table 1. Zr cladding deformation model look-up table [6].

Burst Temperature		Slow-Ramp ($\leq 10^\circ\text{C}/\text{sec}$)		Fast-Ramp ($\geq 25^\circ\text{C}/\text{sec}$)	
$^\circ\text{C}$	K	Burst Strain (%)	Flow Blockage (%)	Burst Strain (%)	Flow Blockage (%)
600	873.15	10	6.5	10	6.5
625	898.15	11	7	10	6.5
650	923.15	13	8.4	12	7.5
675	948.15	20	13.8	15	10
700	973.15	45	33.5	20	13.8
725	998.15	67	52.5	28	20
750	1023.15	82	65.8	38	27.5
775	1048.15	89	71	48	35.7
800	1073.15	90	71.5	57	43.3
825	1098.15	89	71	60	46
850	1123.15	82	65.8	60	46
875	1148.15	67	52.5	57	43.3
900	1173.15	48	35.7	45	33.5
925	1198.15	28	20	28	20
950	1223.15	25	18	25	18
975	1248.15	28	20	28	20
1000	1273.15	33	24.1	35	25.7
1025	1298.15	35	25.7	48	35.7
1050	1323.15	33	24.1	77	61.6
1075	1348.15	25	18	80	64.5
1100	1373.15	14	9.2	77	61.6
1125	1398.15	11	7	39	28.5
1150	1423.15	10	6.5	26	18.3
1175	1448.15	10	6.5	26	18.3
1200	1473.15	10	6.5	36	26.2

The RELAP5-3D cladding deformation model also allows varying hydrodynamic parameters and solutions due to the cladding ballooning and burst. The affected parameters are the flow area, volume, heat transfer hydraulic diameters, flow junction area and hydraulic diameter, and flow junction entrance ratio connecting the volumes.

The rod internal pressure in RELAP5-3D is calculated from the simple static-ideal gas approximation from:

$$P(t) = P(0) \frac{T(t)}{T(0)}$$

where,

$P(t)$ = rod internal pressure at the current time step

$P(0)$ =rod internal pressure at the previous time step

$T(t)$ =temperature of coolant of the reference volume at the current time step

$T(0)$ =temperature of coolant of the reference volume at the previous time step.

The input data needs the initial rod internal pressure and where the reference coolant temperature will be applied. The coolant temperature is selected from the maximum value between the saturation temperature and average gas temperature.

This equation is acceptable for helium or other inert fuel rod gap gases that behave as an ideal gas. One issue is that this equation assumes the rod internal pressure is the only function of adjacent coolant temperature and does not consider the volumetric effect of the fuel rod internals, such as the fuel rod plenum. The fuel rod plenum controls an excessive increase of the rod internal pressure to reduce the potential for fuel ballooning and burst. Since RELAP5-3D is incapable of modeling the fuel rod plenum, it proposes using the coolant temperature at the top of the core part as an alternative solution. The coolant temperature where the plenum is located will be lower than the middle position of the fuel rod since the plenum area does not have the heat source.

When the RELAP5-3D cladding deformation model is activated, related information is automatically printed out to the output file. Below is the example of the cladding deformation related major edit data. The data includes the cladding gap distance, cladding radius, ruptured (i.e., burst) status, and rod internal pressure. Once the fuel rod is ruptured (i.e., burst), the burst time and channel blockage rate is also given along with heat structure node number.

```

0 Str.no. gas gap clad radius ruptured pressure
  m, m, (Pa)
31-001 5.96868E-04 4.95968E-03 no 1.00000E+05
31-002 5.96868E-04 4.95968E-03 no
31-003 5.96868E-04 4.95968E-03 no
31-004 5.96868E-04 4.95968E-03 no
31-005 5.96868E-04 4.95968E-03 no
31-006 5.96868E-04 4.95968E-03 no
31-007 5.96868E-04 4.95968E-03 no
31-008 5.96871E-04 4.95968E-03 no
31-009 2.05459E-03 6.43327E-03 yes
31-010 5.96876E-04 4.95969E-03 no
0---Restart no. 70005 written, block no. 7, at time= 70.0000
--- Restart Write # = 8
1Heat structure 31-009 ruptured at 70.277 seconds with a channel blockage of 21.560 %.

```

To draw graph figures, the user defines minor edit data. The volume quantity AVOL option allows for drawing the flow area change during the simulation. The RELAP5-3D source code was updated to allow users to extract data and draw the gap distance (GAPWD), cladding radius (CLDRAD), and rod internal pressure (PGAP) to make understanding ballooning and burst phenomena easier. This feature will be added to the upcoming version of the RELAP5-3D.

The metal-water reaction model needs to be activated for the accurate cladding deformation modeling. This model allows simulating the initiation of the metal-water reaction near 1000°C and auto-catalytic hydrogen production when the Zr cladding temperature goes over 1200°C (1477 K or 2200 °F). The RELAP5-3D metal-water reaction model was already updated to use two ATFs: Cr-coated Zr and FeCrAl (APMT) [19].

3.2 Verification Test of RELAP5-3D Cladding Deformation Model

3.2.1 Model Description

The nodalization diagram is shown in Figure 7 for the verification test. The model was designed to simulate the cladding ballooning and burst during the LBLOCA dry-out phase; thus, the system is filled with superheated steam due to coolant loss from a ruptured cold leg and the pressure dropped close to the ambient. The model is a vertical pipe with 10 nodes, which represents a single fuel rod subchannel. The pipe length was 1 m (10 nodes of 0.1 m length each) and the area was 0.1 m². The area was set as an arbitrarily large size in order to remove numerical instability from the mass error of the system that resulted from cladding ballooning and burst. The initial pipe condition was set to 0.1 MPa and 600.15 K. The pipe is isothermal, and no heat or flow exchanges through the boundary of the system. The heat structure in the pipe component represents a single fuel rod. Heat generation was uniform throughout the fuel rod except Node 6 where ballooning and burst will occur.

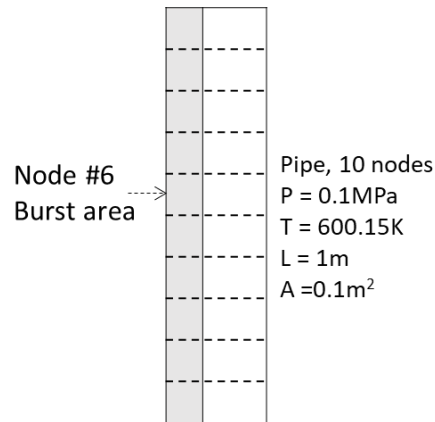


Figure 7. RELAP5-3D nodalization for the cladding deformation test case.

Figure 8 shows the fuel rod nodalization and dimension, which is a typical PWR fuel rod [1].

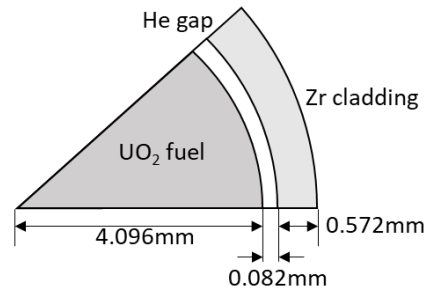


Figure 8. RELAP5-3D fuel rod nodalization and dimension.

The UO_2 fuel has a 4.096 mm radius, and the cladding has 4.178 mm inner diameter and 4.75 mm outer diameter, with a total thickness of 0.572 mm. The gap size was 0.082 mm. Seven nodes were set to UO_2 fuel, one node was set as the He gap, and two nodes were set to Zr cladding. The initial UO_2 fuel temperature was set to 600.15 K. The initial rod internal pressure of the He gap was set to 3.0 MPa. UO_2 and Zr material properties were given by the RELAP5-3D material property data. The properties of He was user input. Metal-water reaction model option was activated to simulate cladding oxidation model with an initial oxide layer thickness of 1 μm .

Four temperature ramp cases were tested for the different interpolation ranges of the RELAP5-3D cladding deformation model by changing the power weighting factor of the pipe component's Node 6: 1, 5, 15, and 27 K/sec.

3.2.2 Results of the Verification Tests

The RELAP5-3D simulation was performed by using a transient calculation with the semi-implicit numerical advancement scheme. The following result is for verification purposes only. The result figures show thermodynamic behavior at Node 6 where cladding deformation occurred.

In general, cladding ballooning and burst time occurred earlier as the temperature ramp rate increases. However, the slope of the temperature increment slightly changed when the ballooning and burst occurred. The reason was that the ballooning and burst increased the fuel rod gap size and thermal resistance, which changes heat transfer behavior. Once large ballooning occurred, the cladding radius and gap width continuously increased until it burst. The rod internal pressure increased proportionally to the coolant temperature and dropped to the ambient pressure (i.e., 0.1 MPa) when the burst occurred.

3.2.2.1 Ramp Temperature 1 K/sec

We selected a ramp temperature of 1 K/sec to verify the cladding deformation model at a very slow temperature rise. The temperature ramp range is $\leq 10^{\circ}\text{C}$ in Table 1. The time step size was 0.01 seconds, and the simulation lasted for 800 seconds.

The cladding formed a large balloon at around 525 seconds and burst at 629.81 seconds with a flow channel blockage rate of 67.376%. The cladding temperature at burst was about 1115 K. The size of the cladding radius and gap width clearly shows the ballooning and burst phenomena in Figure 9.

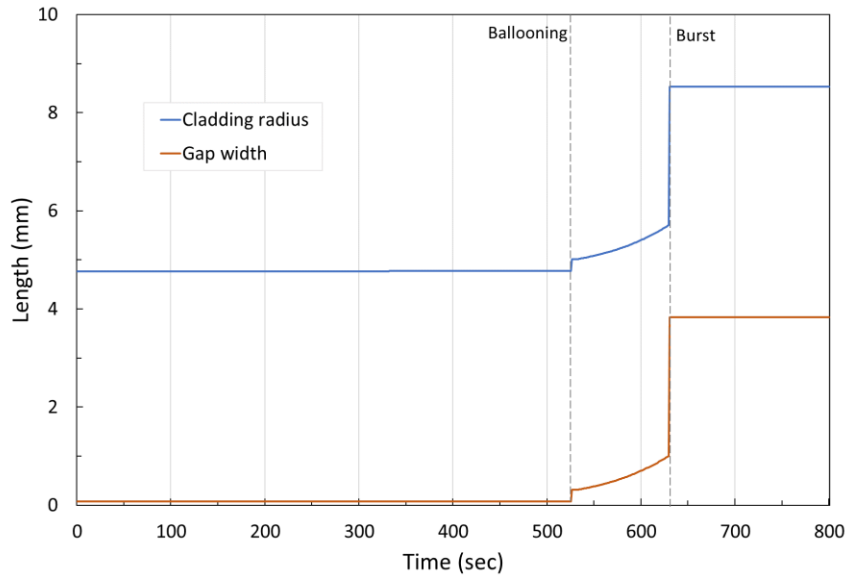


Figure 9. Cladding radius and gap width behavior at Node 6 in the 1 K/sec case.

Figure 10 shows cladding temperature and rod internal pressure behavior at Node 6 where ballooning and burst occurred. The temperature continuously increased after the ballooning and burst occurred, but the slope was slightly changed. The rod internal pressure continuously increased from the start of simulation proportional to the coolant temperature and dropped to the ambient pressure (0.1MPa) when burst occurred.

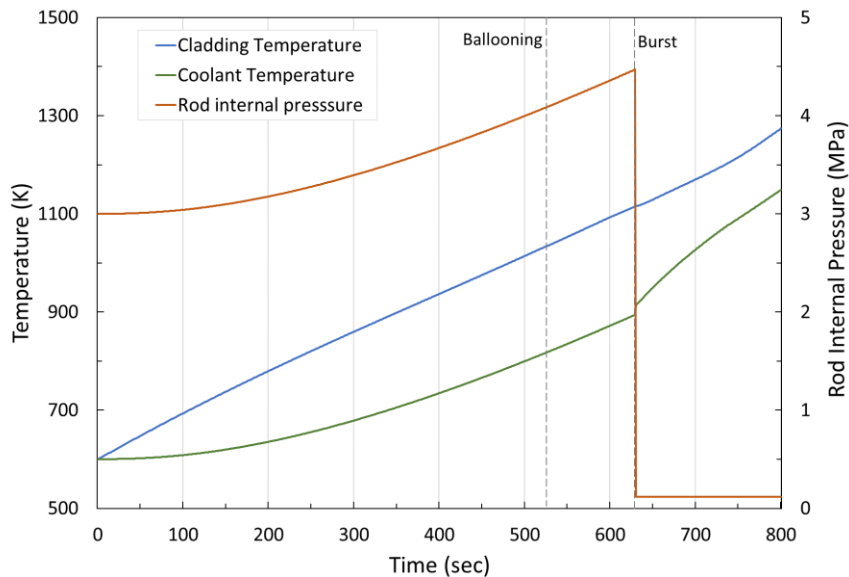


Figure 10. Cladding temperature and rod internal pressure behavior at Node 6 in the 1 K/sec case.

3.2.2.2 Ramp Temperature 5 K/sec

We selected the ramp temperature of 5 K/sec to verify the cladding deformation model at a temperature ramp rate similar to the IFA-650.10 test. The time step size was 0.001 seconds and the simulation conducted for 200 seconds. The temperature ramp range is $\leq 10^\circ\text{C}$ in Table 1.

A large balloon was formed near 103 seconds and burst at 127.32 seconds with a flow area blockage rate of 50.354%. The cladding temperature at burst was around 1151 K.

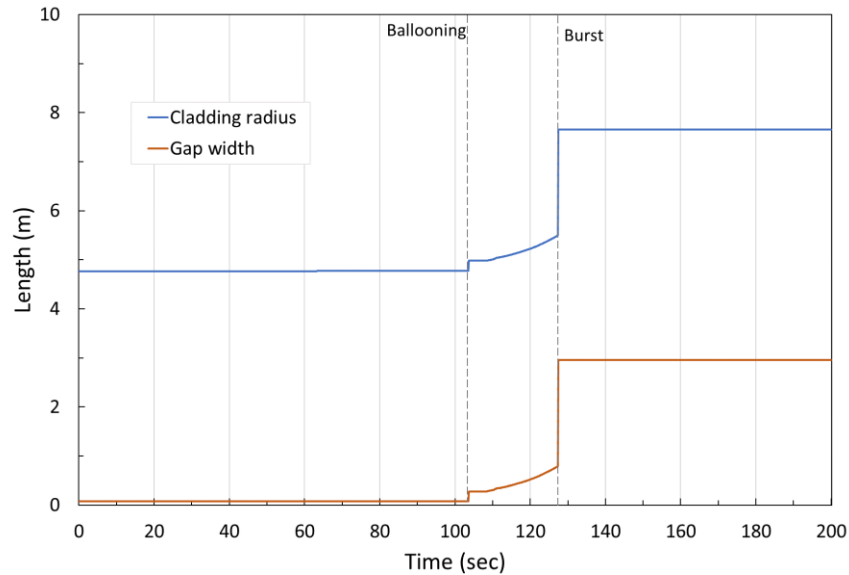


Figure 11. Cladding radius and gap width behavior at Node 6 in the 5 K/sec case.

All the parameters of interest in Figure 11 and Figure 12 show expected result similar to the 1 K/sec case. No specific issue was reported.

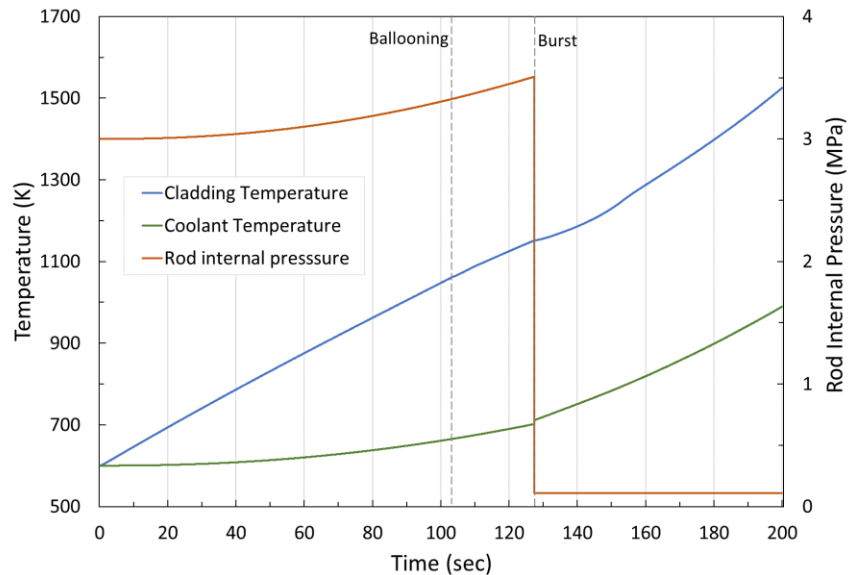


Figure 12. Cladding temperature and rod internal pressure behavior at Node 6 in the 5 K/sec case.

3.2.2.3 Ramp Temperature 15 K/sec

We selected a ramp temperature of 15 K/sec to verify cladding deformation model at moderate temperature rise which is also similar to actual LOCA scenario. The time step size was 0.0001 second, and the simulation lasted 60 seconds. The temperature ramp range is between 10 and 25°C in Table 1.

A large balloon was occurred near 35.5 seconds and burst at 44.758 seconds with a flow area blockage rate of 33.03%. The cladding temperature at burst was around 1177.3 K. All the parameters of interest in Figure 13 and Figure 14 shown as expected. No specific issue was reported.

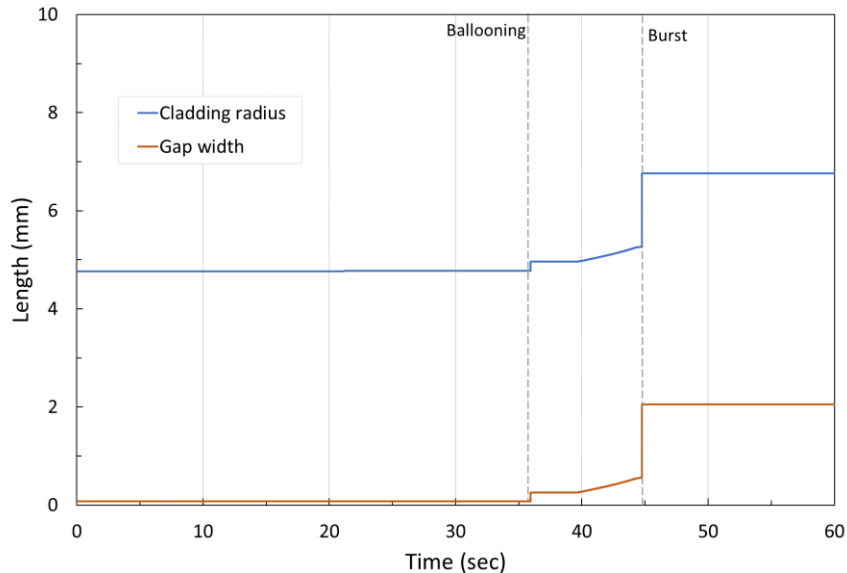


Figure 13. Cladding radius and gap width behavior at Node 6 in the 15 K/sec case.

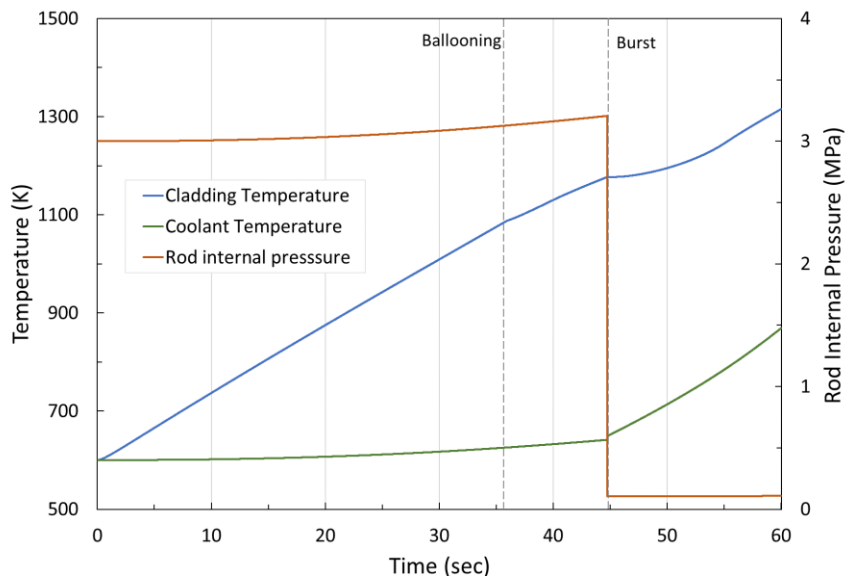


Figure 14. Cladding temperature and rod internal pressure behavior at Node 6 in the 15 K/sec case.

3.2.2.4 Ramp Temperature 27 K/sec

We selected a ramp temperature of 27 K/sec to verify the cladding deformation model at fast temperature rise. The time step size was 0.0001 seconds, and the simulation lasted 30 seconds. The temperature ramp range is $\geq 25^\circ\text{C}$ in Table 1.

A balloon occurred near 18.5 seconds and burst at 24.203 seconds with a flow area blockage rate of 18.115%. The cladding temperature at burst was around 1211 K. All the parameters of interest in Figure 15 and Figure 16 are as expected.

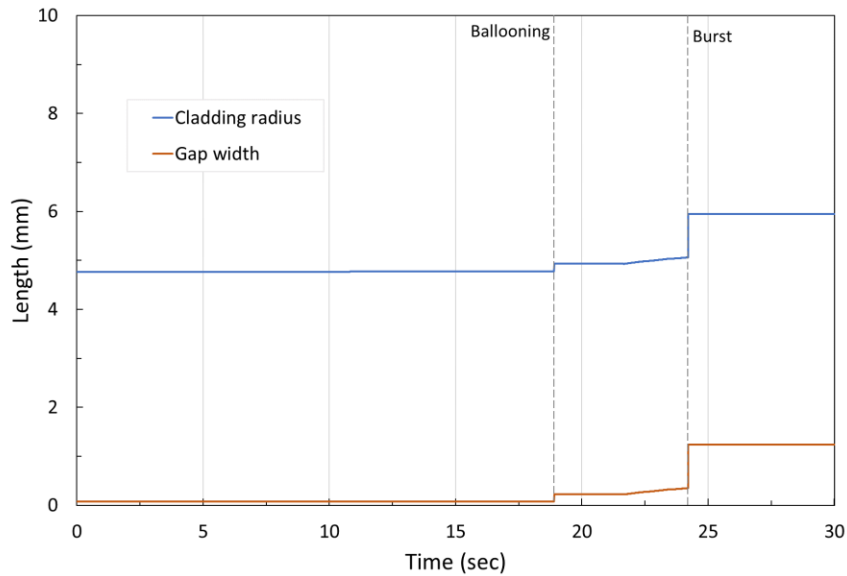


Figure 15. Cladding radius and gap width behavior at Node 6 in the 27 K/sec case.

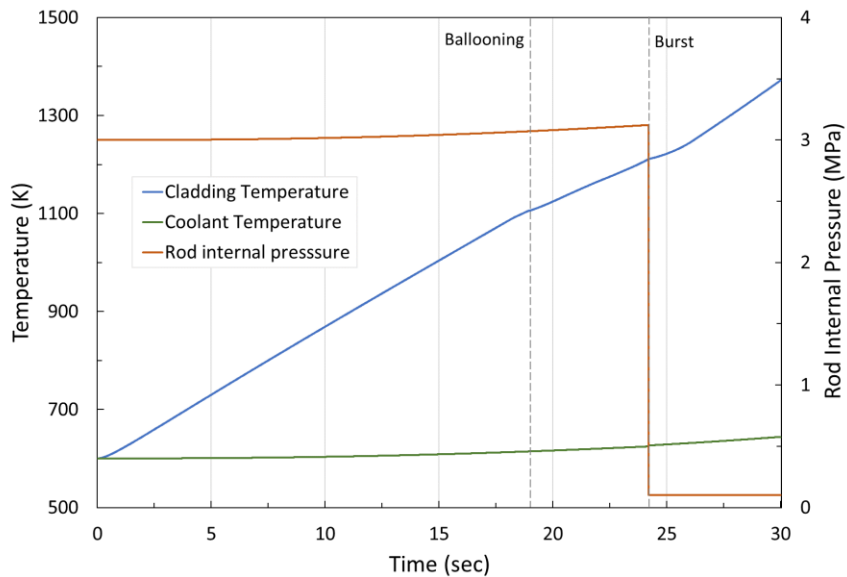


Figure 16. Cladding temperature and rod internal pressure behavior at Node 6 in the 27 K/sec case.

3.2.3 Sensitivity Study on the Time Step Size

The RELAP5-3D input needs two different time step sizes: maximum and minimum. These two different time step sizes are used to find convergence between the space and time discretization. For the thermal-hydraulic problems, it is recommended to use sufficiently small maximum time step size (e.g., 0.01 seconds) to avoid numerical instability during the simulation. However, since RELAP5-3D tends to use the maximum time step first, the result may not represent physical phenomena that may be happen between each time step (e.g., flashing, fast ramping, peaking). Hence, the sensitivity on the time step size is always recommended.

The sensitivity study was conducted for the 5 K/sec temperature ramp case. Three different time step sizes were used: 0.01, 0.005, and 0.001 seconds. Figure 17, Figure 18, Figure 19, and Figure 20 shows cladding temperature, rod internal pressure, flow area change, and mass error, respectively.

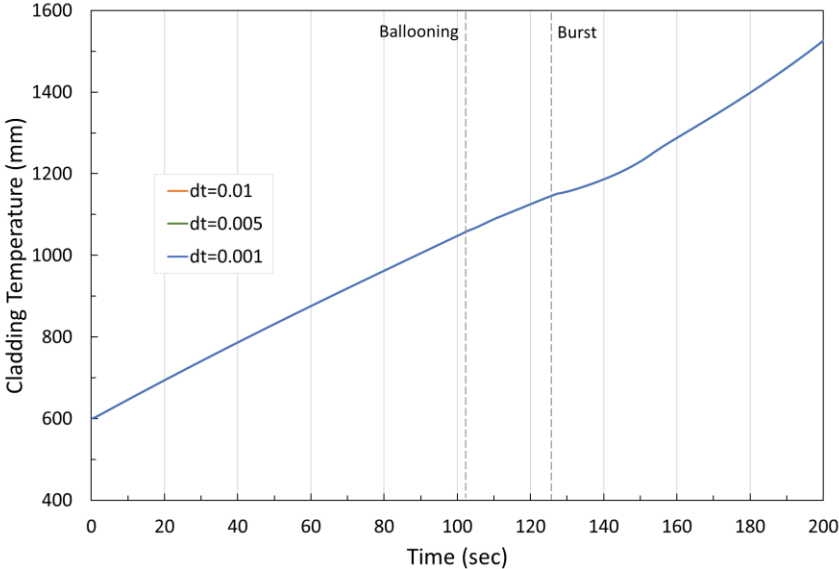


Figure 17. Cladding temperature behavior at Node 6 with different time step sizes.

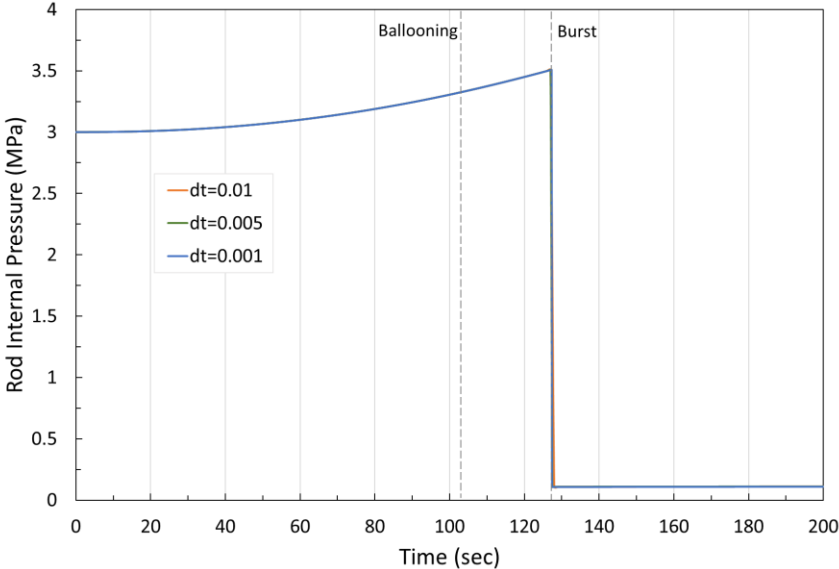


Figure 18. Rod internal pressure behavior at Node 6 with different time step sizes.

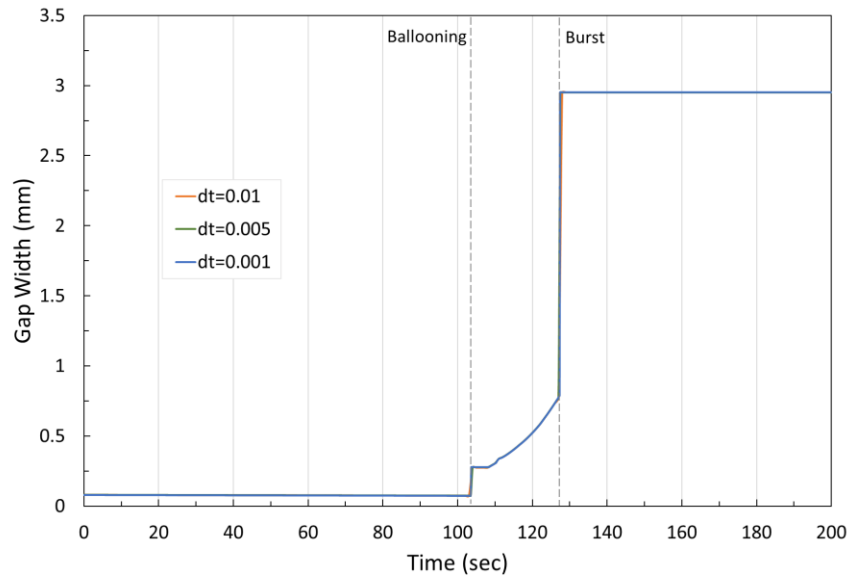


Figure 19. Gap width behavior at Node 6 with different time step sizes.

There is a discrepancy in mass error, as shown in Figure 20. Since the system has a large flow area to remove numerical instability from the mass error, this discrepancy did not affect the physical results. However, if the system has a small volume without the pressure boundary conditions, a large mass error will occur, and the code simulation will fail. In other words, the system volume change due to the cladding deformation may violate the acceptance range of the mass conservation error as time advances in the simulation. RELAP5-3D has an updated model to accept the hydrodynamic change as cladding size changes to minimize the mass error effect. However, this model is not yet verified or validated.

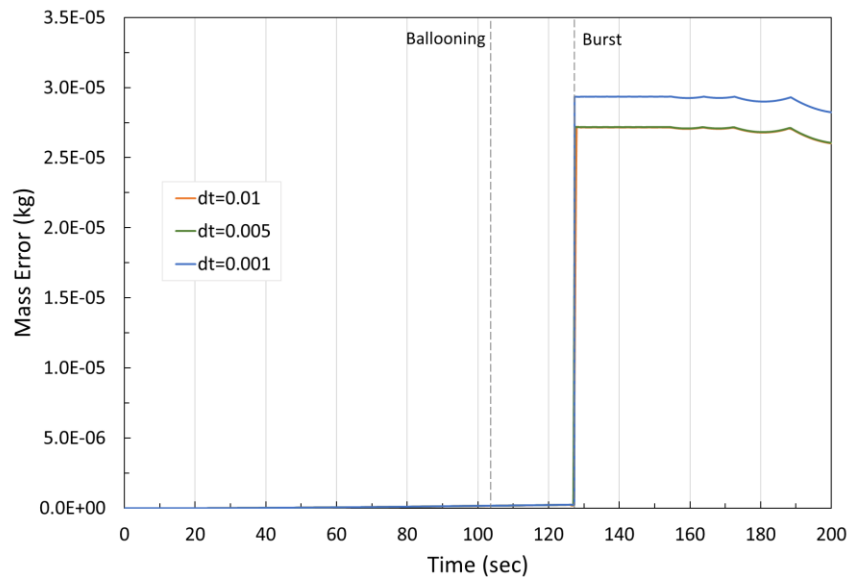


Figure 20. Mass error behavior at Node 6 with different time step sizes.

3.3 Validation of the RELAP5-3D Cladding Deformation Model

3.3.1 Summary of Halden IFA-650 Experiments

The IFA-650 tests are a series of experiments conducted as a part of the Organization for Economic Cooperation and Development Halden Reactor Project to investigate fuel behavior during LOCAs, especially on

the FFRD [7]. The IFA-650 tests comprise both fresh fuel rods and high-burnup fuel rods. The first LOCA experiments using IFA-650.1 were conducted in May 2003 using a fresh, tight-gap, unpressurized PWR fuel rod with low-tin Zr-4 cladding. The IFA-650.2 experiments were carried out in May 2004 using a fresh pressurized PWR rod to practice the test case with ballooning and fuel failure to find out how to run the later experiments with the preirradiated rods. The IFA-650.3/4/5/9/10 experiment series used the preirradiated PWR fuel. The IFA-650.7/12/13/14 experiment series used the BWR fuel, and the IFA-650.6/11 experiment series used the VVER (Water-Water Energetic Reactor: Russian version of PWR) fuel. As shown in Figure 4, in the IFA-650.9/4 case, the fuel pulverized at extremely high burnups (i.e., higher than 90 MWd/kgU) that led to a significant fuel fragmentation and relocation during the LOCA test.

We selected the IFA-650.10 test for the validation of the RELAP5-3D cladding deformation model. The IFA-650.10 used Zr cladding fuel in a commercial PWR (i.e., Gravelines NPP Unit 5, France), irradiated to a burnup around 61MWD/kgU. The burnup level was moderate, and no fuel fragmentation relocation was shown. The parameters of interest for the validation are the cladding temperature and heat-up rate, cladding ballooning size, and cladding burst time.

3.3.2 Description on the IFA-650.10 Test

3.3.2.1 IFA-650.10 Test Rig Geometry

Figure 21 shows the IFA-650.10 test rig description. A preirradiated single fuel rod was inserted into a pressure flask, which is connected to a water loop.

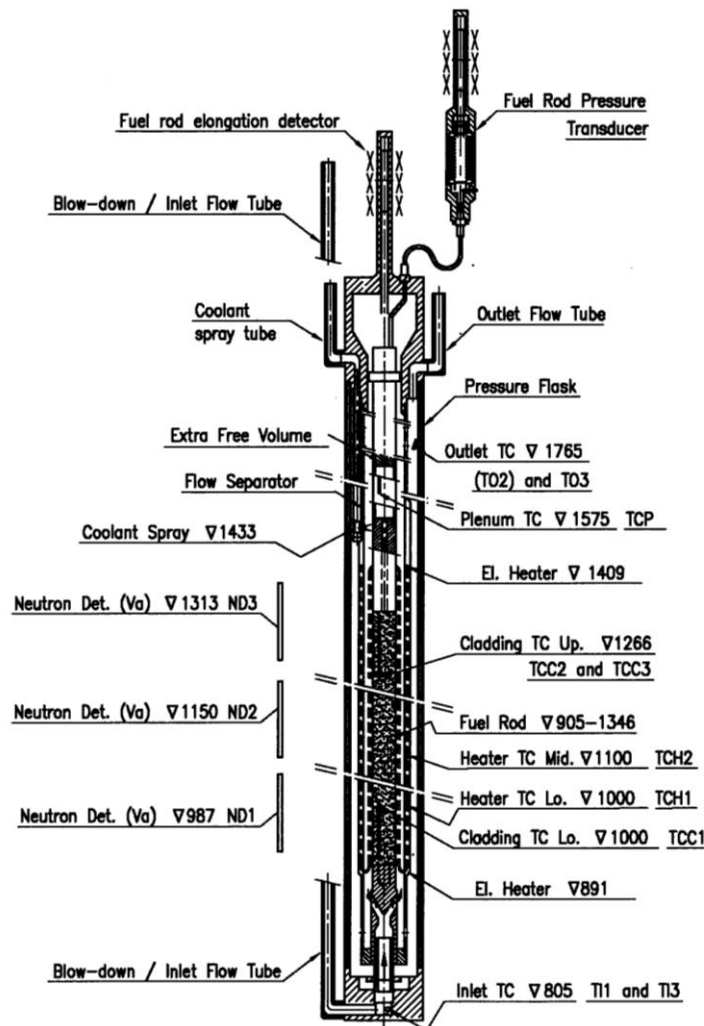


Figure 21. Schematic of the IFA-650.10 LOCA test rig with instrument elevations [8].

The fuel rod was located in the center of the rig surrounded by an electrical heater inside the pressure flask, as shown in Figure 22. The fuel and cladding material were UO_2 and Zr-4, respectively. The refabricated fuel rod was filled with a gas mixture of 95% argon and 5% helium at 40 bar³.

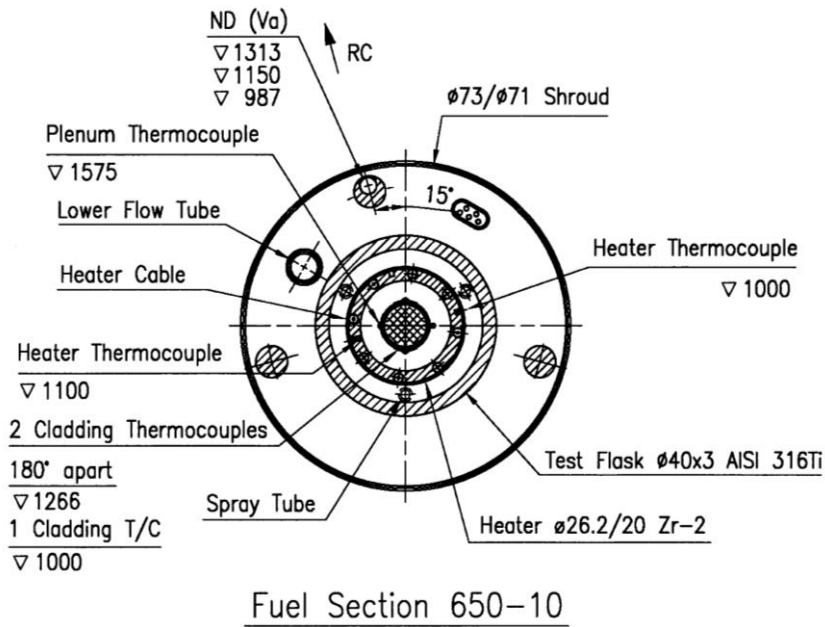


Figure 22. Cross-sectional geometry of the IFA-650.10 rig [8].

The axial power distribution of the fuel rod was symmetric with a peak-to-average power factor of 1.05 as shown in Figure 23.

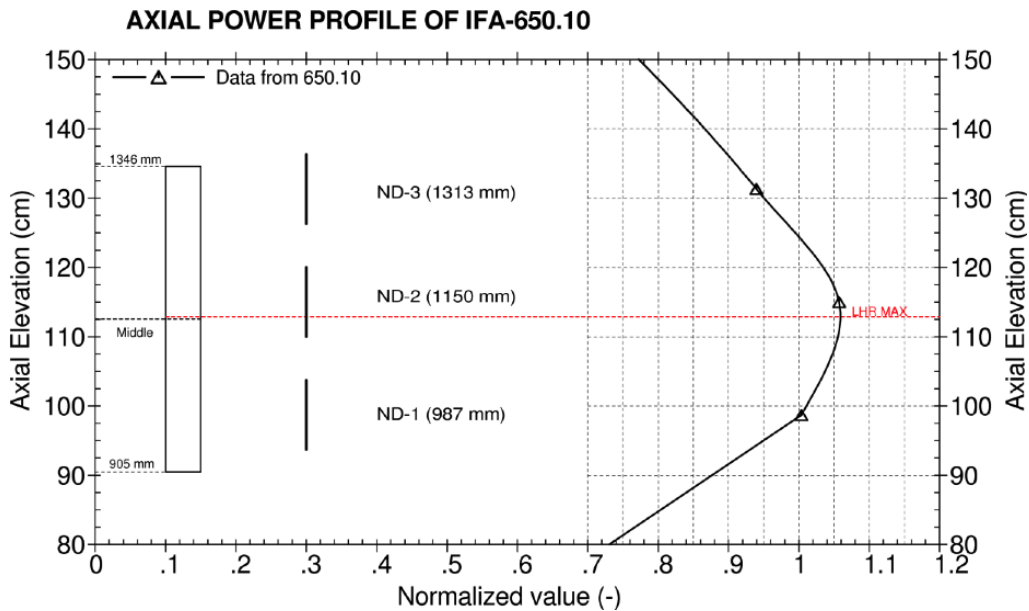


Figure 23. Axial power profile at the beginning of test of IFA-650.10 [8].

³ IFA-650 test series used pressure unit of “bar” instead the standard unit “Pa.” The RELAP5-3D assessment in this report therefore used “bar” to facilitate comparison.

A cylindrical heater was used to simulate heat from the adjacent fuel rods in the actual reactor core. The heater divides the internal space of the rig into an inner annular channel surrounding the fuel rod and outer annulus between the heater and pressure flask. Major design parameters of IFA-650.10 test rig are tabulated in Table 2.

Table 2. Major design parameters of the IFA-650.10 test rig [8].

Part	Length [mm]	Diameter (ID/OD) [mm]	Material
Fuel	440	8.33 (OD)	UO ₂
Cladding	—	8.36 / 9.50	Zry-4
Heater	518	20.00 / 26.20	Zry-2
Pressure flask	—	34.00 / 40.00	AISI 316Ti
Inner shroud tube	—	62.00 / 64.00	Zry-2
Outer shroud tube	—	71.00 / 73.00	Zry-2

The test scheme of IFA-650.10 consists following phases [8]:

- 1) Start-up phase: Steady-state heater operation in 100 W/cm for 3 weeks with the outer loop connected and forced water coolant circulation flow. The system pressure was 70 bars and temperature was around 240°C. Power calibration was made during this period.
- 2) Preparatory phases: A decrease of the linear heat generation rate of the fuel rod to 1.33 kW/m. The outer loop is then removed. The flow separator enabled natural circulation flow in the test section by controlling the flow valves. Full pressure still exists in the rig. The heater was preset to 1.2 kW/m.
- 3) Blowdown phase: Blowdown phase started by releasing water to the dump tank. The channel pressure decreased down to 4 bar.
- 4) Heat-up phase: Stagnant superheated steam surrounding the test pin provided inadequate cooling, and the fuel cladding temperature increased quickly. The target cladding temperature was 850°C and the duration of the temperature transient was 5 minutes (300 seconds) from the end of the blowdown to the scram. Ballooning and burst were expected during the heat-up phase. Spray was applied in 0.5 second pulses with 20 second intervals and was stopped just after cladding failure. Ballooning and burst occurred during the heat-up phase and were detected from pressure and temperature signals.
- 5) After the hold at PCT, the heater was turned off and the test rig was scrammed 418 seconds after the blowdown. There was no spray applied during the cooling down period. The loop was not reconnected to avoid radioactivity contamination.

The RELAP5-3D simulation was focused on the heat-up phase because the main objective of the work is to evaluate the cladding deformation model performance. In this regard, the preparatory and blowdown phases were focused on setting up the proper initial and boundary conditions of the fuel rod. Small amounts of water were periodically sprayed into the rig during the heat-up phase to maintain a sufficient amount of steam for cladding oxidation. This spraying also decreased the cladding, heater, and coolant temperature. However, there is no quantitative information on the water spraying so the explicit modeling of water spraying was not implemented in this work. Instead, the heat generation rate was adjusted to mimic the water spraying effect.

3.3.2.2 Data from the IFA-650.10 Test

Figure 24 and Figure 25 illustrate data generated from the IFA-650.10 test. Time 0 second (T+0) was set as the blowdown initiation. At the beginning of the blowdown phase, the rod internal pressure was near 70 bar. The cladding and heater temperatures decreased during the blowdown phase. The heat-up phase began at T+71

seconds as the rig was practically emptied of water. The fuel ballooning started at T+228 seconds, and the burst occurred near T+249 seconds with 700°C cladding.

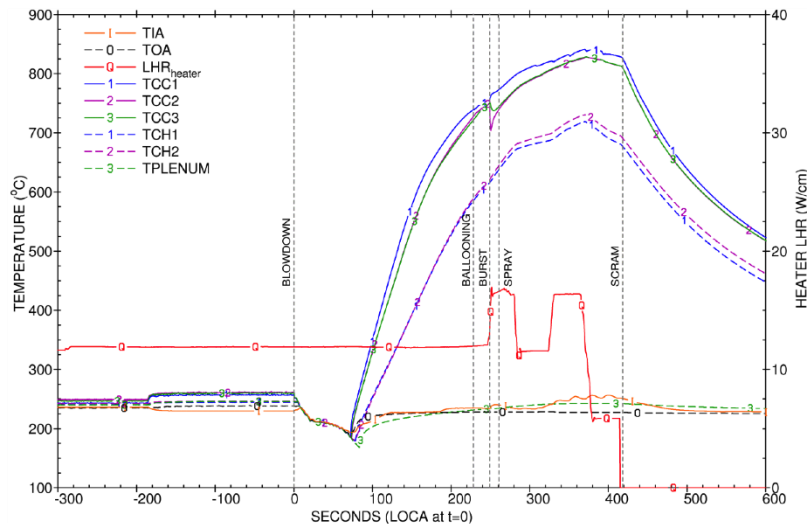


Figure 24. IFA-650.10 Experiment Data Set 1: Temperatures of cladding (TCC), heater (TCH), coolant inlet (TIA) and outlet (TOA) temperatures, and heater power (Heater LHR) [7].

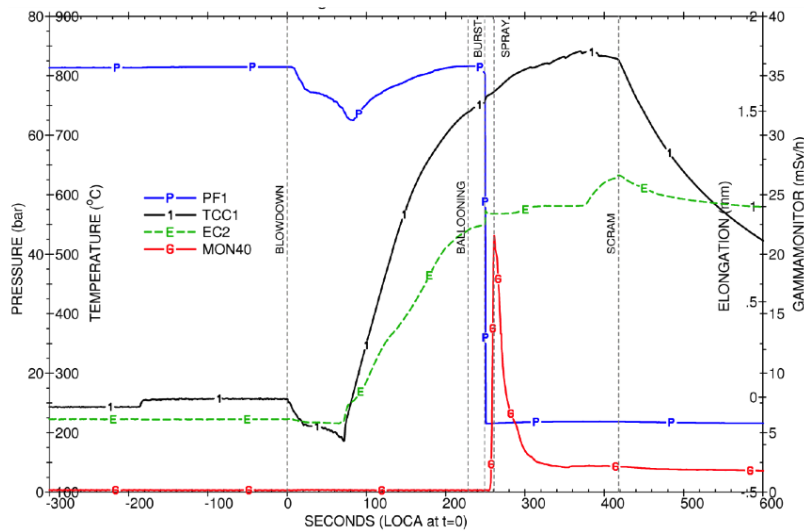


Figure 25. IFA-650.10 Experiment Data Set 2: Rod internal pressure (PF1), cladding temperature (TCC1), rod elongation (EC2), and gamma monitor response in the blowdown line (MON40) [7].

The rod internal pressure decreased during the blowdown phase and increased with the increasing cladding temperature during the heat-up phase. The rod internal pressure rapidly decreased to blowdown tank pressure once the fuel burst occurred. The test was ended by the reactor scram at T+418 seconds. The average cladding heating rate was about 5°C/s for TCC1 and about 4.3°C/s for TCC2 and TCC3.

3.3.3 RELAP5-3D Simulation of the IFA-650.10 Test

3.3.3.1 RELAP5-3D Nodalization

Figure 26 illustrates the overall RELAP5-3D nodalization of the IFA-650.10 test, which is developed based on the test rig geometry shown in Figure 21 and Figure 22. The surrounding equipment were modeled based on previous research [8].

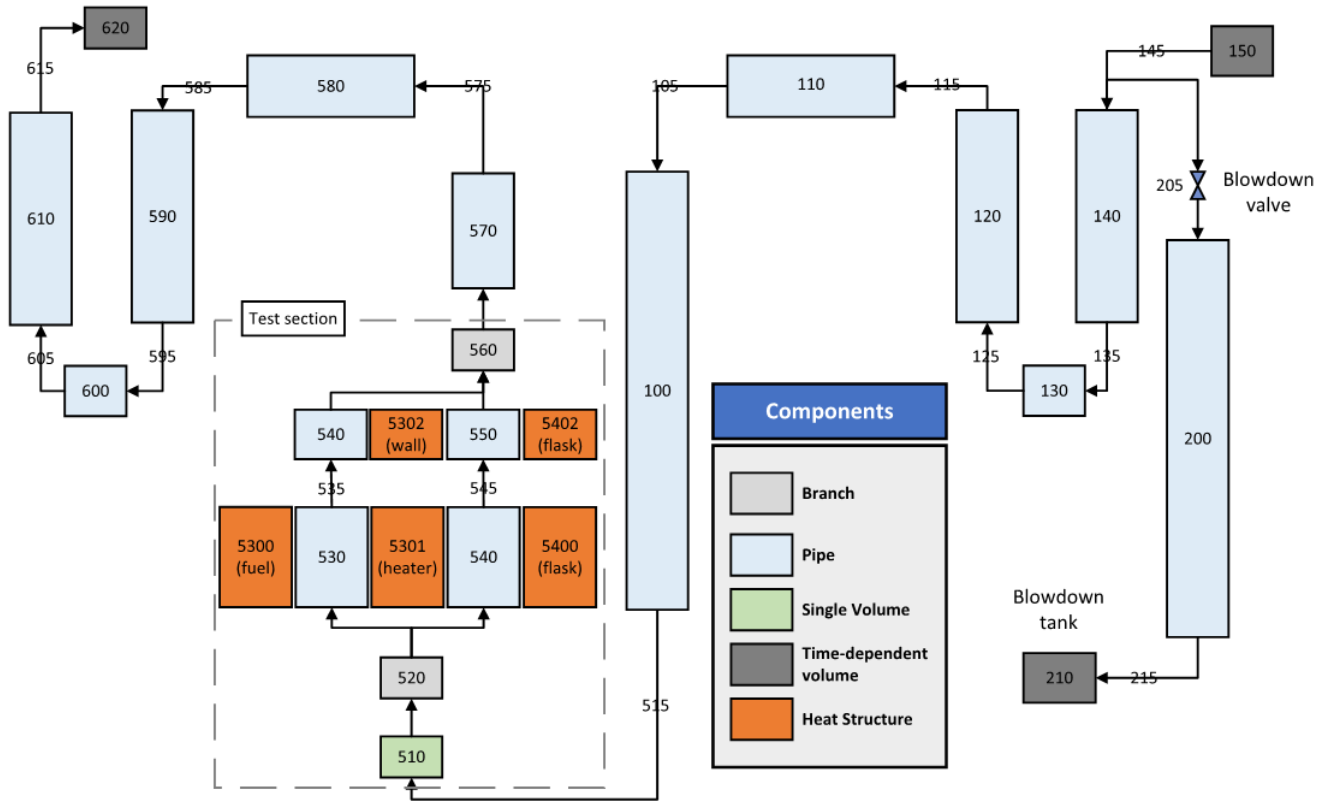


Figure 26. RELAP5-3D nodalization of IFA-650.10.

Figure 27 illustrates detail nodalization information of the core section and the heat structure. The fuel rod (heat structure 5300) consists of 21 axial nodes and seven radial mesh points. The length is 0.44 m and the hydrodynamic diameter of the flow area (pipe 530) is 0.0015m. The heater (heat structure 5301) and lower pressure flask (heat structure 5400) structures have 21 axial nodes and three radial mesh points. For the plenum area, two separate pipes are connected with non-heated wall (heat structure 5302) which allows conduction heat transfer. The upper pressure flask is also modeled (heat structure 5402).

Node 6 corresponds to the lower thermocouple location (TCC1), and Node 18 corresponds to the upper thermocouple location (TCC2 and TCC3) of the test rig.

As shown in Figure 27, the UO_2 fuel has a radius of 4.165 mm and cladding has a 4.75 mm radius and cladding thickness of 0.57 mm. The gap size is 0.015 mm. The initial UO_2 fuel temperature was set to 503.15 K with the initial rod internal pressure of 71.1 bar. The metal-water reaction model option was activated to simulate the cladding oxidation model, which assumed the initial oxide layer thickness was 3 μm .

Time-dependent fuel and heater heat generation rates were implemented in the RELAP5-3D input. During the heat-up phase, the linear heat generation rates of fuel was reported to be 1.33 kW/m. The time-dependent heater heat generation rate was implemented as measured. The pressure flask was modeled as the adiabatic boundary condition. However, due to the lack of necessary data (e.g., temperature, mass flow rate, quality, etc.), the spray system is not modeled. This will result higher fuel cladding temperature and different thermal-hydraulics behavior compared to the experiment. Instead, the heater power profile was adjusted to model spray effect like the other IFA-650.10 benchmarks [31].

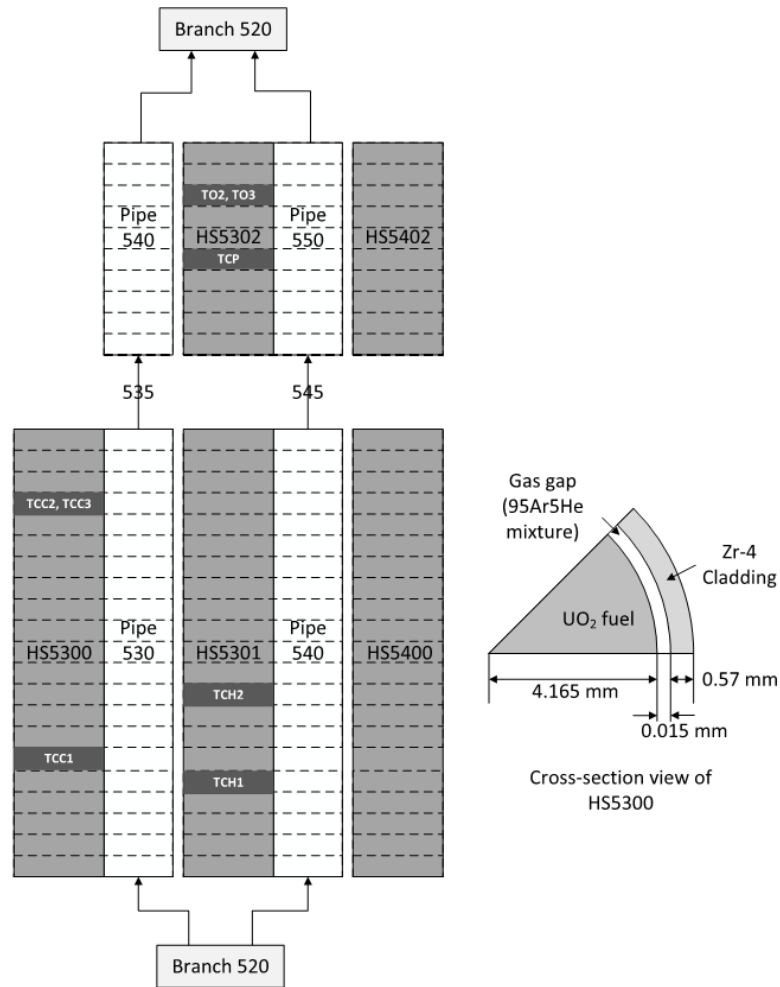


Figure 27. Detailed nodalization of core section of IFA-650.10 test section.

The RELAP5-3D simulation for the IFA-650.10 test was divided into two stages: a steady-state calculation for the start-up and preparation phase from T-200 seconds to set test initial conditions and a transient calculation for the blowdown, heat-up, and cooldown phase. The blowdown phase simulation was begun by opening the trip valve (Component 205) at T+0.1 second. The total simulation time was T+600 seconds. The maximum and minimum time steps of the simulation were 0.001 and 1e-06 seconds, respectively.

In the preparatory phases, Component 530 remained about 193-198°C at 71 bar with the natural circulation mass flow rate of 0.037–0.038 kg/s while the experiment was around 230°C. The cladding temperature of the fuel rod was 193.9°C at Node 6 and 198°C at Node 18 while in the experiment was 256°C (TCC1) and 260°C (TCC2 and TCC3).

For the blowdown and heat-up phases, the components for the boundary conditions for the natural circulation (e.g., Components 150 and 610 and Junctions 145 and 605 in Figure 25) were removed. Once the blowdown was completed, the core section (Component 530 and 540) was filled with superheated steam. In the experiment, the timing of the completion of the blowdown was T+271 seconds. However, due to the lack of detailed information of the blowdown conditions of the experiment, a discharge rate was arbitrarily given to the blowdown valve (Component 205 of Figure 25) to complete blowdown near T+271 by comparing temperature at TCC1 and Node 5 and TCC2 and Node 18.

The radiative heat transfer among the fuel, heater, and pressure flask was implemented in the simulation which is the major heat transfer mechanism as the temperature increases during the heat-up phase. The simulation used an emissivity of 0.6, which is the typical surface emissivity of oxidized Zr cladding [32]. The emissivity of the heater was assumed to be 0.4, which is the typical value of stainless steel [33]. The spray cooling was not modeled due to the lack of information. Instead, the power rate was adjusted to follow experiment temperature profile.

3.3.3.2 RELAP5-3D Simulation Result

The ramp temperature of the IFA-650.10 was about 5°C/s, which is comparable to the verification test case in Section 3.2.2.2. The temperature ramp range is therefore $\leq 10^\circ\text{C}$ in Table 1. The result figures show thermodynamic behavior at Node 14 where cladding deformation occurred. These results are from the blowdown phase. The ballooning started around T+150 seconds and burst at T+197.43 seconds with a flow channel blockage rate of 58.826%. For the rod internal pressure, top of the fuel area (Node 21 of the Component 530: 530-21) was set for the reference flow volume. The power profile was not adjusted in this result; thus, the spray effect was neglected.

Figure 28 shows the cladding temperature and pressure behavior at Node 14. The temperature at burst was about 735°C. A small temperature drop was observed when the ballooning and burst occurred, which was not observed during the verification test in the previous chapter. The main reason was that the temperature increasing slope change due to the ballooning and burst will also be affected by the boundary conditions for the flow channel. During the verification test in the previous chapter, the isothermal boundary condition was used for the flow channel. However, the IFA-650.10 model allows for heat loss from the flow channel by the radiation and natural convection to the connected component. Hence, the heating rate of the test rig needs additional time to recover the thermal resistance from the ballooning and burst, where the temperature temporally drops until it rises again.

The rod internal pressure increased up to 100 bar. When ballooning occurred, the pressure dropped to near system ambient pressure (i.e., 5 bar) as the fuel rod burst. The ballooning and burst timing was identical to the temperature behavior.

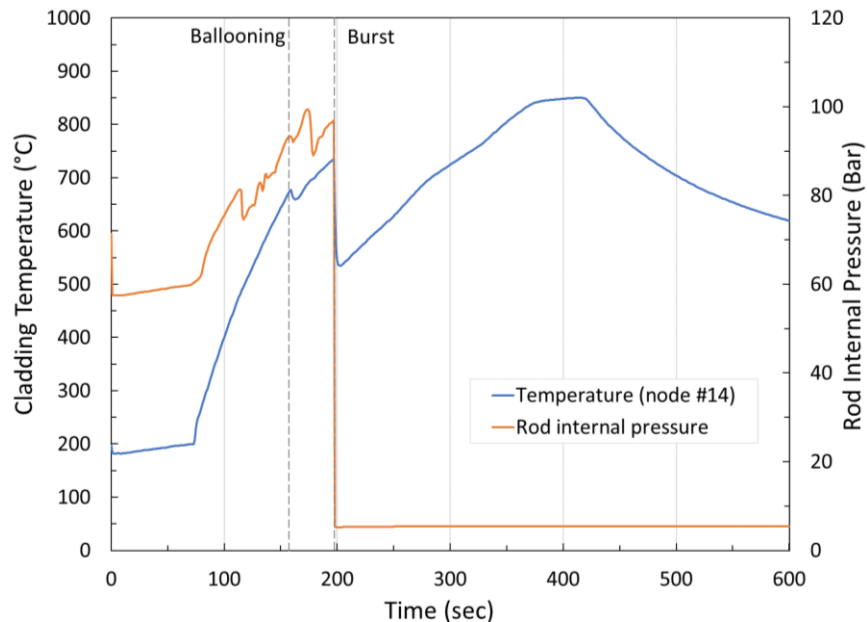


Figure 28. Temperature and pressure behavior at Node 14 of RELAP5-3D IFA-650.10 simulation.

3.3.4 Data Comparison and Discussion

The power profile was adjusted to model the spray effect and compared non-adjusted and experiment data. Figure 29 shows the cladding temperature and pressure at Node 14 with adjusted heat power profile. Same to original power case in previous section, top of the fuel area (Node 21 of the Component 530: 530-21) was used for the rod internal pressure reference volume. The ballooning started near T+180 seconds and burst at T+248.63 with the blockage rate of 66.673%. The reference flow volume is set for the top node of Component 530 (i.e., 530-21) for the rod internal pressure. The temperature at burst was about 753°C.

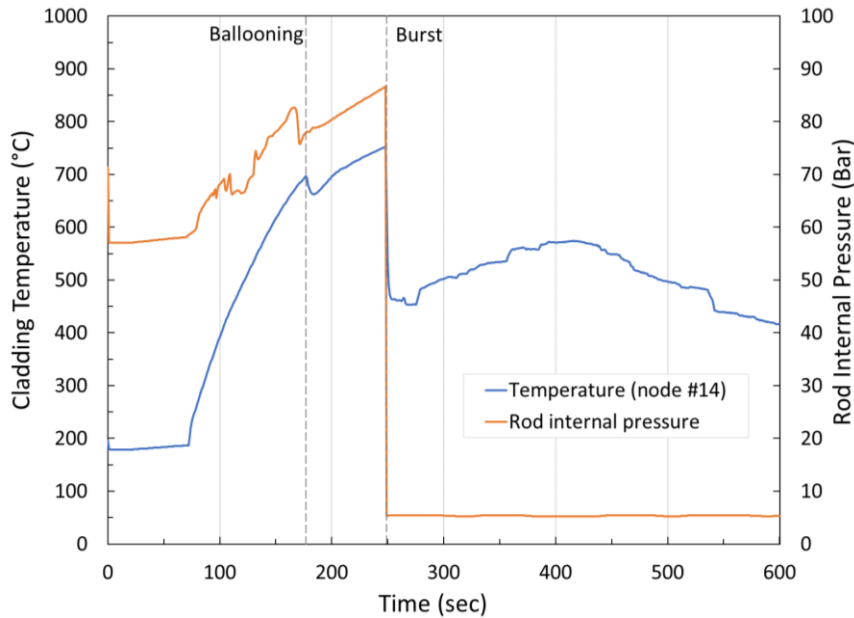


Figure 29. Temperature and pressure behavior at Node 14 of RELAP5-3D IFA-650.10 simulation (power adjusted).

Table 3 shows the time sequence comparison between the RELAP5-3D simulation and the experiment. With power adjusted the burst time of the RELAP5-3D simulation is comparable to the experiment. However, starting time of the ballooning is still earlier than the experiment.

Table 3. Time sequence of the IFA-650.10 RELAP5-3D simulation result.

Event	RELAP5-3D (sec)	RELAP5-3D power adjusted (sec)	Experiment (sec)
Start-up phase	T-200	T-200	T-200
Initiation of blowdown	T+0.1	T+0.1	T+0
End of blowdown	T+75	T+75	T+71
Start of heat-up	T+75	T+75	T+71
Ballooning	T+150	T+180	T+228
Burst	T+197.43	T+248.63	T+249
Scram and cooldown	T+418	T+418	T+418
End of simulation	T+600	T+600	T+600

Figure 30 and Figure 31 show the cladding and heater temperature comparison between the experiment and the RELAP5-3D simulation at lower (TCC1 and Node 6) and higher (TCC2 and Node 18) elevation. The temperature behavior in the RELAP5-3D simulation with the adjusted power generally agreed with the experiment.

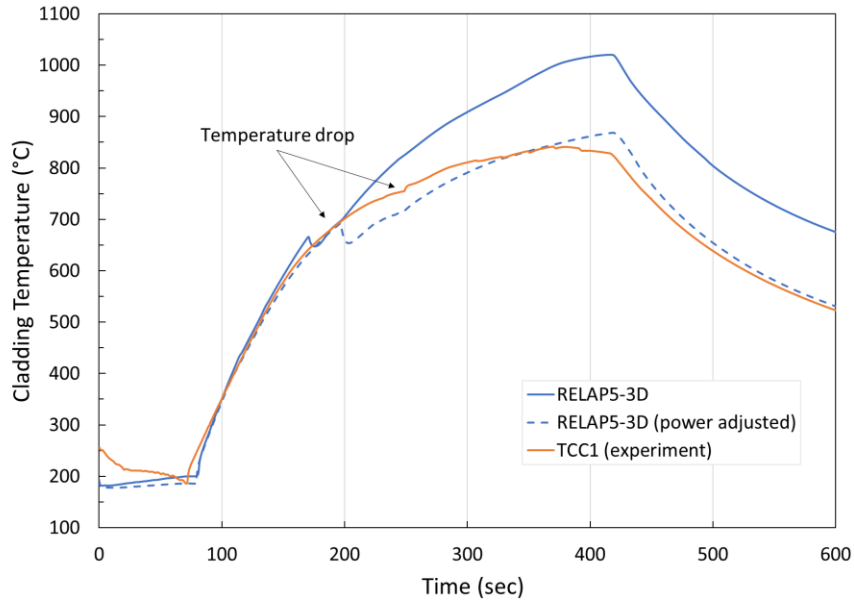


Figure 30. Lower elevation cladding (TCC1 and Node 6) cladding temperatures comparison.

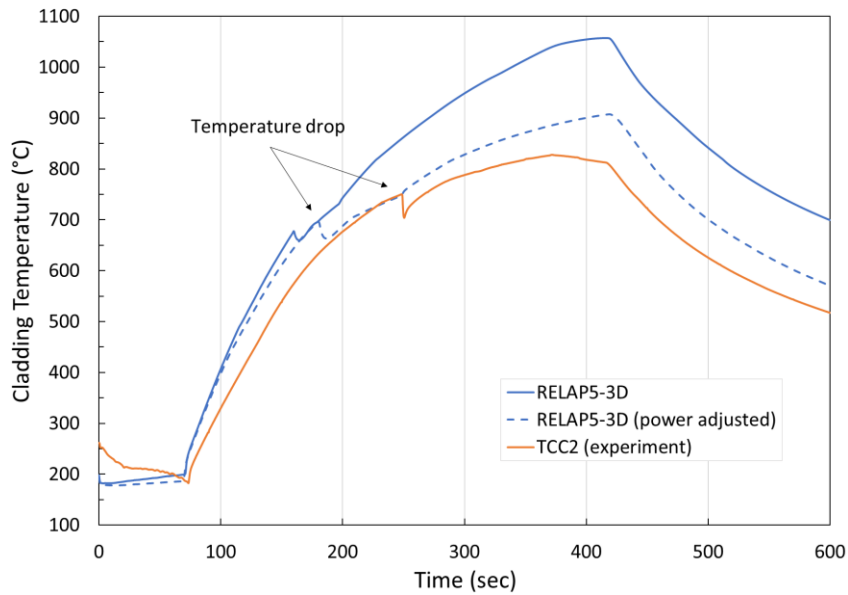


Figure 31. Higher elevation cladding (TCC2 and Node 18) cladding temperatures comparison.

The burst position predicted by the RELAP5-3D code was Node 14, which is close to the experiment as shown in Figure 32. With the adjusted power, the burst size became larger since the blockage rate was increased from 58.826% to 66.673%.

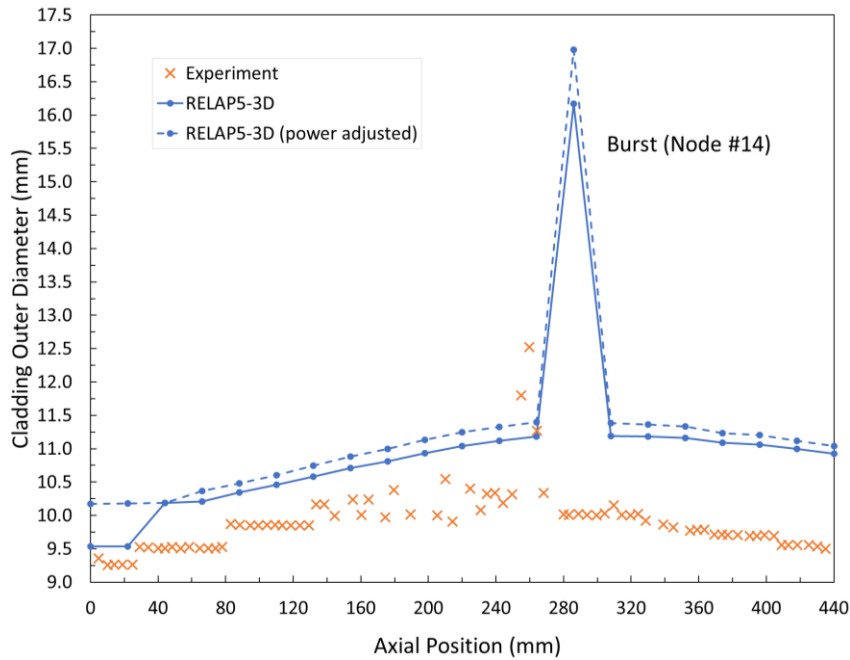


Figure 32. Comparison of burst position using cladding outer diameter.

Figure 33 shows comparison of the rod internal pressure of the experiment (PF1) and RELAP5-3D. With power adjusted RELAP5-3D simulation is more comparable to the experiment, but still shows discrepancies between the experiment.

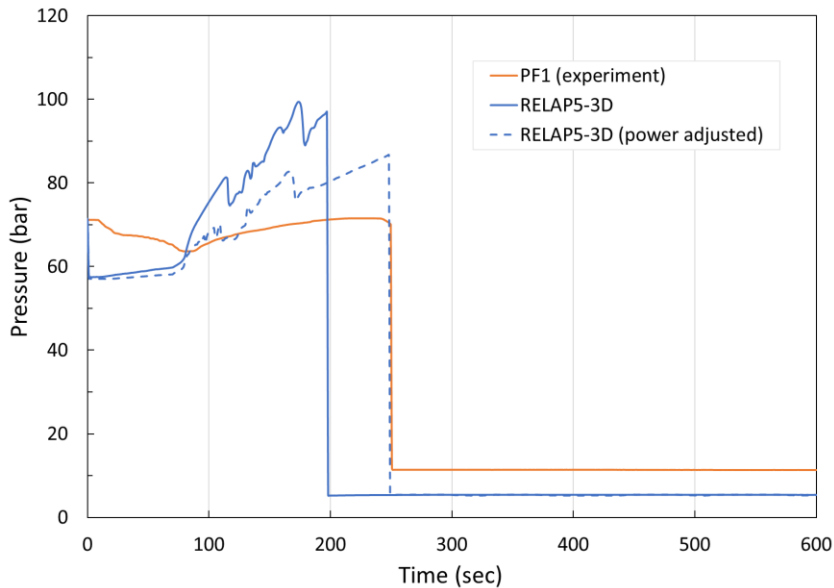


Figure 33. Comparison of the rod internal pressure.

The main reason was from the methodology used in the RELAP5-3D to model the rod internal pressure. As described in Section 3.1, the RELAP5-3D cladding deformation model uses simplified static pressure equation. The behavior of the rod internal pressure follows the behavior of the vapor temperature of the reference fluid volume where user defined. In other word, the rod internal pressure can be changed based on the user's definition of the reference fluid volume. As an example, Figure 34 shows the effect of reference fluid volume to the rod internal pressure. The pressure behaviors are inconsistency when referring top of the fuel area (Node 21

of the Component 530: 530-21) and bottom of the plenum area (Node 1 of the Component 540: 540-01) which are adjacent each other. It is therefore recommended to use fuel rod performance simulation tool to predict accurate rod internal pressure when the burst occurred during RELAP5-3D simulation.

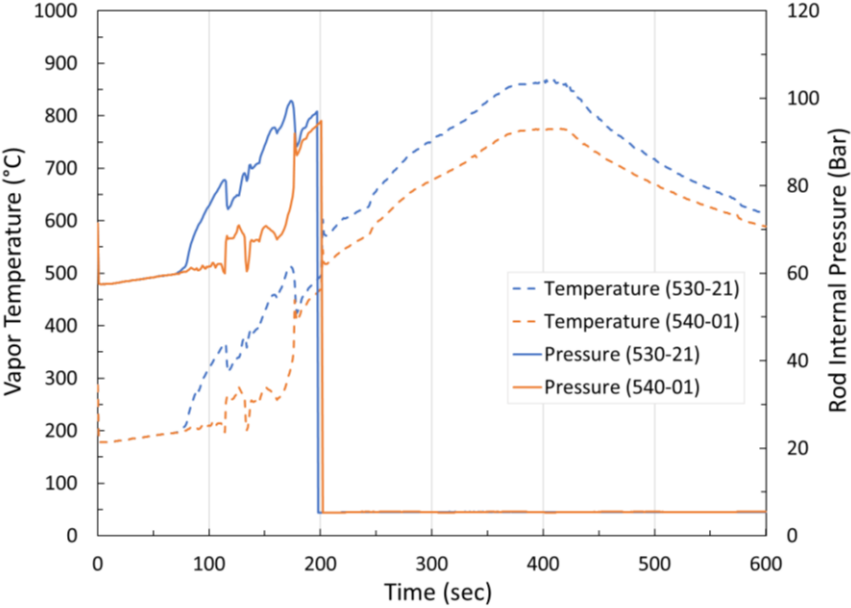


Figure 34. RELAP5-3D rod internal pressure comparison with different reference volume.

4. CONCLUSION AND REMARK

The main technical issues in the modeling and simulation of the HBU ATF are from insufficient experimental data to support developing simulation tools and correlations and conducting verification and validation. Some experimental data is available in material properties or mechanical characteristics. However, the majority of experiments need at least several years to reach HBU and be useful in a database. Beside a lack of experimental data, the major issues in modeling and simulation of HBU ATF are that:

- 1) The cladding deformation model is limited to Zr cladding at LOCAs,
- 2) A multi-dimensional approach is recommended to simulate cladding deformation,
- 3) FFRD phenomena of Cr-coated Zr cladding needs high-fidelity simulation tools,
- 4) Modeling and simulation need to consider the 10% higher CHF value of FeCrAl cladding.

The RELAP5-3D cladding deformation model can provide a quick snapshot information of potential fuel failure during a LOCA analysis through its own cladding deformation model. It is however recommended that standalone fuel performance analysis code simulation is necessary to confirm details of the fuel failure mechanism. The RELAP5-3D cladding deformation model is conservative since the model does not consider the fuel rod plenum and leads to a rapid pressure increase, which is an important parameter to the ballooning and burst earlier than expected. The model uses predefined stress and strain correlations and look-up table for Zr cladding, which has a maximum temperature limit of 1200°C. The rod internal pressure behavior follows the static-ideal gas model, which is proportional to the adjacent coolant temperature. This may cause systematic uncertainties, and model revision will improve the quality of the outcome. The metal-water reaction model needs be activated when cladding deformation is used. The code was updated to produce graphical data related to the cladding deformation.

The RELAP5-3D cladding deformation model was built only based on Zr alloy cladding material, thus, the model will not be valid for other cladding materials. A new model needs to be developed for the RELAP5-3D application of the ATF loaded system with an HBU operation fuel cycle. The metal-water reaction model for FeCrAl (APMT) and Cr-coated Zr cladding were developed but still need verification and validation. For the ATFs with an HBU operation fuel cycle, RIA needs to be considered as a major DBA since HBU fuel rod behavior can accelerate FFRD and cladding deformation.

No specific issues were found during the verification of the RELAP5-3D cladding deformation model. The model correctly depicts expected physical phenomena by using correlations and look-up table interpolation. The hydrodynamic parameters were correctly varied as flow area changed due to cladding deformation, but an additional assessment is needed for the mass error due to the cladding deformation. From the result of the time step sensitivity study, a sufficiently smaller time step is needed to observe heat flux peaks, which only appear within the very short period of time.

The validation of the RELAP5-3D cladding deformation model was performed using IFA-650.10 test data. The RELAP5-3D results with adjusted heater power were generally comparable to the IFA-650.10 experimental data. The temperature behaves similar to that in the experiment but the ballooning timing was earlier than in the experiment since the RELAP5-3D cladding deformation model is known to be conservative. An issue was found in the rod internal pressure behavior. The fuel rod of the IFA-650.10 has upper plenum which increases the fuel rod internal volume and makes for a slower pressure increase. However, the rod internal pressure in RELAP5-3D only follows the vapor temperature where user defined and cannot model the fuel rod plenum through its own heat structure and fuel models. This made for a smaller fuel rod internal volume and induces higher pressure increase during the simulation. Revising the simplified rod internal pressure calculation model considering the fuel rod internal plenum will reduce systematic uncertainties of RELAP5-3D.

5. REFERENCES

- [1] Y-J. Choi et al. 2022. “Safety Analysis for Accident-Tolerant Fuels with Increased Enrichment and Extended Burnup.” INL/RPT-22-68581, Idaho National Laboratory.
- [2] J-S. Kim, J-D. Hong, Y-S. Yang, and D-H. Kook. 2017. “Rod internal pressure of spent nuclear fuel and its effects on cladding degradation during dry storage.” *Journal of Nuclear Materials* 492: 253–259. <https://doi.org/10.1016/j.jnucmat.2017.05.047>.
- [3] F. J. Erbacher and S. Leistikow. 1985. “A Review of Zircaloy Fuel Cladding Behavior in a Loss-of-Coolant Accident.” KFK-3973, Institut für Materialforschung and Institut für Reaktorbauelemente. <https://doi.org/10.5445/IR/270021792>.
- [4] T. Tram et al. 2020. “A sensitivity study of physical models using in RELAP5 code based on FEBA experimental data.” *Nuclear Science and Technology* 10. <https://doi:10.53747/jnst.v10i4.12>.
- [5] US. NRC. 1980. “Cladding Swelling and Rupture Models for LOCA Analysis.” NUREG-0630, NRC.
- [6] Idaho National Laboratory. 2018. “RELAP5-3D[®] Code Manual Volume 1: Code Structure, System Models and Solution Methods.” INL/MIS-15-36723, Revision 4.4, Idaho National Laboratory (Limited access to data license holders).
- [7] OECD Nuclear Energy Agency. 2016. “Report on Fuel Fragmentation, Relocation, and Dispersal.” NEA/CSNI/R(2016)16, OECD Nuclear Energy Agency.
- [8] A. Lavoil. 2010. “LOCA Experiments IFA-650.10.” Technical Report EP-1650.10, OECD Halden Reactor Project (Limited access to data license holders).
- [9] US. NRC. 2022. “Regulatory Framework Applicability Assessment and Licensing Pathway Diagram for the Licensing of ATF-Concept, Higher Burnup, and Increased Enrichment Fuels.”
- [10] K. J. Geelhood. 2019. “Fuel Performance Considerations and Data Needs for Burnup above 62 GWd/MTU: In-Reactor Performance, Storage, and Transportation of Spent Nuclear Fuel.” PNNL-29368, Pacific Northwest National Laboratory.
- [11] N. Capps et al. 2021. “A Critical Review of High Burnup Fuel Fragmentation, Relocation, and Dispersal under Loss-Of-Coolant Accident Conditions.” *Journal of Nuclear Materials* 546, 152750. <https://doi.org/10.1016/j.jnucmat.2020.152750>.
- [12] US. NRC. 2021. “Phenomena Identification Ranking Tables for Accident Tolerant Fuel Designs Applicable to Severe Accident Conditions.” NUREG/CR-7283, NRC.
- [13] OECD Nuclear Energy Agency. 2022. “State-of-the-art Report on Nuclear Fuel Behaviour Under Reactivity-initiated Accident Conditions (RIA SOAR).”
- [14] D. Kamerman et al. 2020. “High-burnup Experiments in Reactivity Initiated Accidents (HERA).” INL/EXT-20-57844, Idaho National Laboratory. <https://doi.org/10.2172/1874819>.
- [15] Idaho National Laboratory. “A Finite Element-Based Nuclear Fuel Performance Code.” <https://mooseframework.inl.gov/bison/index.html>.
- [16] C. Folsom et al. 2016. “BISON Modeling of Reactivity-Initiated Accident Experiments in a Static Environment.” *Top Fuel 2016*, Boise, ID, September 11–16, 2016. <https://www.osti.gov/servlets/purl/1358206>.
- [17] C-Y. Jin, J. Lee, and D-Y. Oh. 2020. “Validation of Integrated Code of MARS-KS and FRAPTRAN Using Halden IFA-650.5 LOCA Test.” *Transactions of the Korean Nuclear Society Virtual Spring Meeting*, July 9–10, 2020.
- [18] Y-J Choi et al. 2022. “Development of Plant Reload Optimization Platform Capabilities for Core Design and Fuel Performance Analysis.” INL/RPT-22-70382, Idaho National Laboratory.

- [19] C. Parisi et al. 2019. “Risk-Informed Safety Analysis for Accident Tolerant Fuels.” *Nuclear Science and Engineering* 194. <https://doi.org/10.1080/00295639.2020.1732699>.
- [20] X. Wu and K Shirvan. 2020. “System Code Evaluation of Near-term Accident Tolerant Claddings during Boiling Water Reactor Short-term and Long-term Station Blackout Accidents.” *Nuclear Engineering and Design* 356: 110362. <https://doi.org/10.1016/j.nucengdes.2019.110362>.
- [21] F. Qi et al. 2020. “Pellet-cladding mechanical interaction analysis of Cr-coated Zircaloy cladding.” *Nuclear Engineering and Design* 367: 110792. <https://doi.org/10.1016/j.nucengdes.2020.110792>.
- [22] J. Yang et al. 2022. “Review on chromium coated zirconium alloy accident tolerant fuel cladding.” *Journal of Alloys and Compounds* 895: 162450.
- [23] Y. Lee, J-I Lee, and H. C. Noh. 2017. “Mechanical analysis of surface-coated zircaloy cladding.” *Nuclear Engineering and Design* 49(5): 1031–1043. <https://doi.org/10.1016/j.net.2017.03.012>.
- [24] N. Capps et al. 2018. “PCI analysis of Zircaloy coated clad under LWR steady state and reactor startup operations using BISON fuel performance code.” *Nuclear Engineering and Design* 332: 383–391. <https://doi.org/10.1016/j.nucengdes.2018.03.045>.
- [25] F. Qi et al. 2020. “Pellet-cladding mechanical interaction analysis of Cr-coated Zircaloy cladding.” *Nuclear Engineering and Design* 367: 110792. <https://doi.org/10.1016/j.nucengdes.2020.110792>.
- [26] Y. Lee and T. Kim. 2022. “Enhancement of Void Predictability of System Code by Applying Inter-Channel Turbulent Mixing Model in Bundle.” *The 19th International Topical Meeting on Nuclear Reactor Thermal Hydraulics (NURETH-19)*, Brussels, Belgium, March 6–11, 2022.
- [27] C. Grandjean. 2005. “A State-Of-The-Art Review of Past Programs Devoted to Fuel Behavior Under LOCA Conditions. Part One. Clad Swelling and Rupture. Assembly Flow Blockage.” IRSN, SEMCA-2005-313.
- [28] D. G. Groeneveld et al. 2007. “The 2006 CHF look-up table.” *Nuclear Engineering and Design* 237: 1909–1922. <https://doi.org/10.1016/j.nucengdes.2007.02.014>.
- [29] M. Liu et al. 2017. “Potential impact of accident tolerant fuel cladding critical heat flux characteristics on the high temperature phase of reactivity initiated accidents.” *Annals of Nuclear Energy* 110: 48–62. <https://doi.org/10.1016/j.anucene.2017.06.016>.
- [30] S. C. Resch et al. 1982. “FRAP-T6: The Transient Fuel Rod Behavior Code.” NUREG/CR-2950, Idaho National Engineering Laboratory.
- [31] OECD Nuclear Energy Agency. 2010. “Benchmark Calculations on Halden IFA-650 LOCA Test Results.” NEA/CSNI/R(2010)6, OECD Nuclear Energy Agency.
- [32] J. Stuckert. 2002. “On the thermo-physical properties of Zircaloy-4 and ZrO₂ at high temperature.” Technical Report FZKA 6739, Kernforschungszentrum Karlsruhe. <https://doi.org/10.5445/IR/270052940>
- [33] F. P. Incropera and D. P. DeWitt. 1996. *Fundamentals of Heat and Mass Transfer 4th Edition*. New York City, New York, John Wiley & Sons, Inc.